Adapting Solid Oxide Fuel Cell to Operate on Landfill Gas; Breaking C-C Bonds on a Nickel Anode

by

Sandra Boakye

Submitted in Partial Fulfillment of the Requirements

for the Degree of

Master of Science

in

Chemistry

YOUNGSTOWN STATE UNIVERSITY

August, 2024

Adapting Solid Oxide Fuel Cell to Operate on Landfill Gas; Breaking C-C Bonds on a Nickel Anode

Sandra Boakye

I hereby release this thesis to the public. I understand that this thesis will be made available from the OhioLINK ETD Center and the Maag Library Circulation Desk for public access. I also authorize the University or other individuals to make copies of this thesis as needed for scholarly research.

Signature:

_____

Sandra Boakye, Student Date

Approvals:

_____

Dr Clovis Linkous, Thesis Advisor Date

_____

Dr Timothy Wagner, Committee Member Date

_____

Dr Josef Simeonsson, Committee Member Date

_____

Salvatore A. Sanders, PhD, Dean, College of Graduate Studies Date

ACKNOWLEDGEMENT

I am grateful to God Almighty for his protection and abundant grace he showed me and made this master's degree a success. I would like to thank the faculty of the Department of Chemistry and Youngstown State University for the scholarships provided during my education and stay in the USA. I appreciate the assistance and guidance given me by Dr Clovis Linkous and my committee members during my research work.

My profound gratitude goes to the Boakye family and friends especially Lisa Devore from the Department of Chemistry as well Mrs Mazi, for their love, encouragement and support given to me through out these years. Finally, I would like to thank anyone who accepted and welcomed me to their homes especially members of friends around the world, Evangel Baptist church and PIWC.

ABSTRACT

Solid oxide fuel cells (SOFCs) are high temperature electrochemical devices that convert chemical energy stored in fuels to electricity. The SOFC has numerous benefits, such as its fuel flexibility, higher efficiency and low carbon emissions. However, the SOFC suffers major drawbacks, such as low cell performance over time due to poisoning caused by impurities, leading to deactivation and loss of catalytic activity of the anode materials. In this study, voltametric experiments were conducted with an SOFC made of 8 mol% yttria-stabilized zirconia (YSZ) as an electrolyte, nickel anode, lanthanum strontium manganite (LSM) cathode, and with platinum electrodes. The Pt/YSZ/Pt and Ni/YSZ/LSM cell buttons were made by painting the cells with the appropriate inks and heated for six to eight hours in an oven at 1000 ºC. The cells were fixed on a Probostat^{TM} using Ceramabond and air dried for one to four hours. The Probostat^{TM} was placed in a furnace and heated up to 750 ºC. The Ni/YSZ/LSM cell exhibited higher cell performance as compared to Pt/YSZ/Pt cell with the passage of humidified hydrogen. Scanning Electron Microscopy (SEM), Energy Dispersive Spectroscopy (EDS) and X-Ray Diffraction (XRD) were conducted on control and coated YSZ substrates painted with electrode materials. The Ni/YSZ/LSM cell showed 66.78 atomic percent oxygen, 16.35 % nickel, and 13.96 % zirconium, which was consistent with the cermet anode composition. Ultra-high purity methane and propane gases were humidified and passed through the Ni/YSZ/LSM cell at a flow rate of 50 ml/min, and then voltage-current curves obtained. There was higher cell performance in propane as compared to the methane gas. Images obtained after the experiment showed a black deposit on the anode, and EDS analysis indicates the presence of 97.09 % carbon. It was evident that water vapor at 0.66 atm was insufficient to prevent carbon deposition via pyrolysis of propane at 750 ºC.

TABLE OF CONTENTS

LIST OF FIGURES

LIST OF TABLES

CHAPTER ONE

INTRODUCTION

For any work to be carried out, mechanical, electrical or chemical, an energy requirement needs to be supplied into the system or object under consideration. Energy exists in the sun as solar energy, whilst energy stored in atoms and organic matter as chemical energy can be useful in the generation of electricity. There are two forms energy, namely renewable and non-renewable energy. Non-renewable energy, such as coal, natural gas, petroleum, and nuclear energy cannot be replaced when they are used up. Fossil fuels release carbon dioxide during combustion, which traps infrared radiation leading to greenhouse effect and global warming.[1] Despite the deleterious effects of fossil fuels, there is still a high demand for them. As a result, there has been a drop in the natural fossil fuels in the world due to higher dependence. Therefore, if appropriate measures are not put in place, the world is going to run out of fossil fuels very soon. [2]

In attempt to address this issue, there has been a need to look out for alternative, renewable and sustainable forms of energy. [3] Green energy is a renewable, ecofriendly, and cheaper alternative of energy production, whilst clean energy sources have lower carbon emissions. Fuel cells are devices that convert chemical energy stored up in fuels into electricity by redox mechanisms. A fuel cell is composed of electrodes (anode and cathode) and electrolyte as shown in Fig 1.1. The setup is then connected to wires and an external load. Oxidation of fuel occurs at the anode whilst the oxidant, usually air, is reduced at the cathode.[4] If hydrogen is used as fuel, the by-product of the redox mechanism is water, which does not contribute to environmental pollution making it a greener alternative. However, if fuels such as natural gas are oxidized, there is a possibility of generating less

carbon dioxide and monoxide, hence making it a clean energy source. According to White and Oleikseiwiez, fuel cells have several applications including energy storage, transportation, and generation of electricity.[5]

FUEL CELLS

According to Gasik, fuels cells are electrochemical devices that operate by redox process to generate electricity. There are five forms of fuels cells, namely solid oxide fuel cells, phosphoric acid fuel cells, alkaline fuel cells, polymer electrolyte membrane fuel cells and molten carbonate fuel cells.[6] Phosphoric acid and alkaline fuel cells operate at lower temperatures, hence require the use of catalysts to improve their efficiencies, and ultimately makes the cells costly to use as a form of generating electricity. Besides, there is a tendency for the contents of the cells to be corroded because the electrolyte used is in solution form at low and high pH, respectively.

Solid oxide fuel cells (SOFCs) are a form of modern electrochemical cells and have received much attention. This is primarily due to their greater energy efficiency as compared to combustion engines.[7] According to Zhang and Hu, the importance of SOFCs include the usage of different sources of fuel, lower costs, and little or no pollution.[8] SOFCs are used in manufacture of electric vehicles, generation of electricity and aerospace technologies.

In solid oxide fuel cells (SOFCs), the electrolyte employed is a solid ceramic material, usually yttria-stabilized zirconia (YSZ), gadolinia-doped ceria or samarium-doped ceria. Zirconium dioxide is unstable and undergoes a phase transition at 1173 K from cubic to tetragonal. Upon addition of yttrium oxide (Y_2O_3) to ZrO_2, the cubic structure is retained.[9] YSZ has low membrane permeability, great chemical stability and high ability

to transport ions at elevated temperatures (800-1000 ºC) making it a preferred electrolyte for solid oxide fuel cells. [10]

There are several metals and perovskites that are used to produce the electrodes. For anode materials, the metals used could be manganese, iron, cobalt, nickel, platinum and ruthenium. NiO-YSZ cermet is used but during the operation of the SOFC, NiO is reduced to Ni. Nickel is mostly used due to high fuel oxidation and electron conduction properties. The cathode is usually made from lanthanum strontium manganite and lanthanum strontium cobalt ferrite. [11]

DIAGRAM OF SOLID OXIDE FUEL CELL

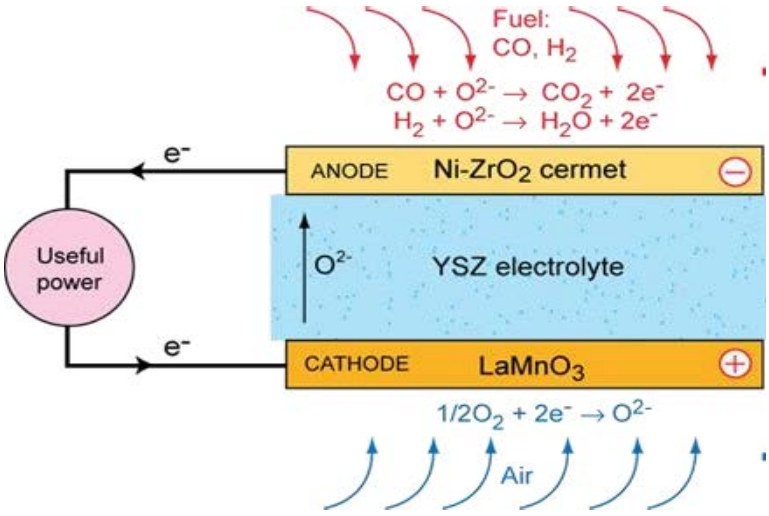

Fig 1.1: Diagram of fuel

https://www.doitpoms.ac.uk/tlplib/fuel-cells/high_temp_sofc.php

STEAM OR INTERNAL REFORMING OF METHANE AND PROPANE GAS ON NICKEL ELECTRODES

The reactions below summarize what chemistry can occur when small hydrocarbons, such as methane and propane, are reacted with water:

1a. $CH_4 + H_2O \rightarrow CO + 3H_2$

1b. $CO + H_2O \rightarrow CO_2 + H_2$

1c. $CH_4 + 2H_2O \rightarrow CO_2 + 4H$

1d. $C_3H_8 + 6H_2O \rightarrow 3CO_2 + 10\ H_2$

CHEMICAL EQUATIONS REPRESENTING REACTIONS OCCURRING IN SOFC ANODE

The following steps summarize what electrochemistry may occur when molecular hydrogen, methane, or solid carbon are oxidized at an SOFC anode:

2. $H_2 + O^{2-} \rightarrow H_2O + 2e^-$

3a. $CH_4 + 4O^{2-} \rightarrow CO_2 + 2H_2O + 8e^-$

3b. $CH_4 + 3O^{2-} \rightarrow CO + 2H_2O + 6e^-$

3c. $CH_4 \rightarrow C + 2H_2$

3d. $C + 2O^{2-} \rightarrow CO_2 + 4e^-$

CATHODE REACTION – UPTAKE OF O_2 TO BECOME LATTICE OXIDE

4. $O_2 + 4e^- \rightarrow 2O^{2-}$

STATEMENT OF PROBLEM

Generally, SOFCs operate at very high temperatures between 800 -1000 ℃ and the energy requirements to supply this amount of heat are extremely high so scientists are looking at means of modifying SOFCs to work at lower temperatures and maintain higher efficiencies. Large-scale production of SOFCs has been limited due to the microstructural and chemical changes in electrodes during the electrochemical process. SOFCs can be operated using a wide range of fuels including landfill gases (LFG). The constituents of LFG tend to poison electrodes and reduce the overall performance as well as the life span of the cell. [12]

At extremely high temperatures, there is a possibility of strontium ions diffusing from the cathode material (LSM) and entering the electrolyte. Sr combines with YSZ and forms $SrZrO_3$. This transforms YSZ from a stable cubic to an unstable tetragonal structure leading to phase degradation. [13] High temperatures lead to thermal expansion of electrodes and contraction if cooled to lower temperatures. This leads to microcracking on the surface of the electrode and delamination. [14]

The presence of boron in the LFG reacts with cathodes to form $LaBO_3$, which insulates the three - phase boundary and prevent reaction between the electrodes, electrolytes and the gases thereby deteriorating the cell performance. [15]

The presence of hydrogen sulfide in the fuel even in minute quantities is damaging to the SOFCs. H_2S can react with the anode material to form sulfides or may be further oxidized to SO_2 and H_2SO_4. This leads to corrosion of the contents of the cell. Moreover, there is presence of SO_2 in the air used as an oxidant in the SOFC. Wang et al, reported that SO_2 can react with strontium oxide, which is a major component of the cathode (LSM

and LSCF). This forms $SrSO_4$, which decreases the cell performance especially at higher concentrations of SO_2.[16] Silicon dioxide from siloxanes forms an impermeable membrane on the surface of the anode reducing the electrooxidation process and hence impeding the flow of electrons.

Previous works conducted in Professor Linkous's laboratory by Zivak, Dogho and Baderuddin indicated that the presence of siloxanes, carbon compounds and hydrogen sulfide decreased cell efficiency and electrochemical performance in a matter of seconds.[17,18,19]They concluded that the LFG must be subject to a pretreatment process before running on the SOFC. In addition, Dogho revealed the presence of rubidium metal from SEM/EDS analyses of Ni/YSZ anode ran on Mahoning valley LFG, which could be a possible contaminant leading to cell degradation.[18] Moreover, the results of Dogho showed higher amounts of carbon deposits on the nickel anode after passage of landfill gas, which choked the cell in a matter of minutes.

There are several factors that cause anode deactivation, and these include the temperature, type of anode material, water to hydrocarbon ratio, carbon oxygen ratios as well as composition and concentration of impurity in the fuel. According to Boldrin et al. the fuel with high sulfur and aromatic hydrocarbons content was found to decrease cell efficiency.[20] The presence of hydrocarbons was found to cause coking, which covers the triple phase boundary, blocks the passage of gases, wear out the anode and creation of cracks leading to irreversible damage to the nickel electrode. Therefore, this research will seek to assess the effects of breaking C-C bonds on the deactivation of nickel electrode. To achieve this, the experiment will be carried out in several steps which include:

a. Surface and structural studies on coated and uncoated electrodes using XRD, SEM and EDS.
b. Preparation of platinum electrodes on YSZ and running them on hydrogen versus air, as well as humidified methane and propane gases
c. Preparation of Ni/YSZ and LSM electrodes and running with hydrogen air mixture as well as humidified methane and propane

MICROSTRUCTURE OF SOFC

The surface of the electrodes is made of porous layers, which are permeable to gases whereas the electrolyte enables the conductivity of ions. The SOFC microstructure refers to porosity and size of particles or atoms used in the manufacture of electrodes. There is a direct correlation between particle size and electrode porosity. Ni-YSZ cermet usually has a large surface area and small particle size, which increases its catalytic activity, diffusion of gases and transfer of electrons. Triple phase boundary (TPB) is a region where anode, electrolyte and cathode meet. The Ni-YSZ cermet forms extensive connections into the TPB which allows faster transfer of oxide ions, electrons and gases, therefore enhance the electrochemical performance.[21] Studies conducted by Koide et al. Wilson and Barnet, and Laguna-Bercero, have demonstrated the smaller particle size of nickel increases catalytic activity, conductivity and eventually overall electrochemical performance of the SOFC.[22, 23,24]

Microstructural degradation is affected by size of particles in the electrode, temperature, fuel water ratio, and permeability of the electrodes to diffusing gases. Heenam et al. reported that the microstructure of the nickel electrodes is subject to degradation, which can be attributed to thermal and chemical processes. The thermal process is

primarily due to melting and mismatch in thermal expansion coefficients of nickel during its operation at elevated temperatures (1455 ºC). At this temperature, the atoms in nickel clump together due to the melting process, which tends to minimize cell efficiencies. To prevent agglomeration, there is formation of Ni-YSZ cermet. YSZ is used because of its high melting point at 2700 ºC, which aids in delaying the melting of the nickel anode.[11]

Another approach to preventing the agglomeration process is by using NiO as anode material but this is eventually reduced to nickel metal, leading to melting and agglomeration. This effect exposes the surface of electrodes to degradation by chemical impurities from the fuel such as sulfur, metals, siloxanes and carbon by creation of an insulation layer at the three-phase boundary (TPB), which is situated 10 - 20 μm away from the anode/electrolyte interface. According to Vafaeenezhad et al. 2022, the region within TPB, where the electrochemistry takes place is termed as anode functional layer (AFL). [25] TPB is a region where the electrolytes, electrodes and gases meet, allowing electrochemical reactions to proceed.[26] The formation of an insulation layer will prevent the movement of ions and molecules within the cell components.

Large scale commercialization of SOFCs has not been achieved due to high temperatures required for operation (800-1000 ºC) as well as microstructural, interconnects and sealant degradation. To improve cell efficiencies, microstructural degradation by these impurities in landfill gas needs to be controlled by synthesis of new materials that are resistant to degradation such as ceria oxides, humidification, adsorption and other treatment processes to eliminate the impurities.

DEGRADATION AT THE CATHODES

The cathode can also be exposed to microstructural and chemical degradation because of the presence and deposition of impurities such as chromium ions. Chromium ions are diffused into the cell from the interconnects where they chemically react with the cathode and cause poisoning. [27] Chromium (III) oxide can be reduced into chromium atoms which have the tendency react with the cathode to form $SrCrO_4$ which then insulates the TPB and distort the normal functioning of the cell. They prevent the diffusion and catalytic reduction of oxygen into ions hence reduce electrical conductivity of the cell.

Cathodic overpotential occurs because of presence of other cations which have different rates of migration and cause internal separation of the cathodic materials. These cations react with species such as water and carbon dioxide which later deposits on the surface of cathode and act as insulators. Sakai et al. have reported that the presence of water vapor in air which is used as an oxidant in SOFCs decreased the overpotential of the cathode.[28]Cathodes can be made from perovskites (ABX_3) which are capable of adsorbing carbon dioxide onto their surfaces. There is competition between the carbon dioxide and oxygen gas which prevents the catalytic reduction of oxygen into oxide ions there by decreasing cell efficiencies.

Lanthanum strontium manganite (LSM) is a doped perovskite material used in the construction of cathodes. During the operation of the SOFC, strontium oxide diffuses from the cathode to the surface, covering the TPB and decreasing the current and voltage of the cell. Peng et al. reported that the use of lanthanum strontium manganite as cathode material can react with YSZ to form $La_2Zr_2O_7$ at high temperatures. The $La_2Zr_2O_7$ is an insulator which increases ohmic resistance and reduces electrical conductivity, thereby decreasing

cell efficiency.[28] The air passing through the cathode may contain SO_2, which reacts with the material used to manufacture the cathode. This causes corrosion of the cathode leading to degradation. [29]

DEGRADATION AT THE ANODES

This is a phenomenon by which molecules are attracted to surfaces by physical or chemical processes. The anode has the tendency to adsorb impurities onto its surface, which tend to be mostly irreversible in nature. Studies conducted by Peng et al. have proven that minimal concentrations of hydrogen sulfides adsorbed onto the surfaces of nickel electrode can poison the anode. At high concentrations of sulfur and phosphorus, these impurities form a eutectic mixture with nickel electrodes and lower the melting points and its oxidative potentials. This usually occurs at high temperatures as well.[29]

SOFCs usually operate at high temperatures between 800 -1000 ºC so when fuels containing higher proportions of carbon dioxide and methane are used to run the cells, there is the possibility of the carbon content to be broken down into coke and deposit on the nickel electrodes. Carbon deposition reduces the electrocatalytic oxidation of fuels by nickel, thereby lowering cell efficiencies. Perovskites materials as mentioned earlier have higher affinities for carbon dioxide and reacts chemically with it to form carbonates. Carbonates insulate the nickel electrodes and prevent conduction of electrons, thereby minimizing current.

Borosilicate is used as a sealant in SOFCs. At elevated temperatures used for the operation of the fuel cell, boron is transformed into BO_2 and $B_3H_3O_6$. These boron compounds are volatile and migrate, reacting with lanthanum in the cathode to form an impermeable layer made of $LaBO_3$. This is deposited on the TPB by chain growth

mechanism and prevent diffusion as well as electrocatalytic oxidation of fuels at the anode.[14]

Research conducted by Sasaki et al. showed the reactivities of various halides and metals on electrode surfaces. These metals are present in lesser concentrations in landfill gas but contribute to increases in ohmic resistance and reductions in cell efficiencies. Based on this research, highly reactive metals that can be damaging to electrodes include arsenic, antimony, mercury, selenium, tellurium, germanium, bismuth, germanium, phosphorus, tin, magnesium and alkali metals.[15] These volatile metals may be present in organic forms (mono, di and tri-methylated) forms as well as the inorganic or hydride forms.

Hackett explained that metals are categorized into three based on their volatilities and vapor pressures. The least volatile metals usually settle at the bottom with ash, so they do not collect in the coal syn gas. Ba, Ce, Cs, Mg, Mn, and Th are classified into Group 1. Group 2 metals such as As, Cd, Cu, Pb, Sb, Se, Zn are slightly volatile and associated with particulates. The highly volatile metals such as Hg exist in the vapor phase and end up in coal syn gas.[30] During a cyclic exposure test of selenides in coal syngas conducted by Hackett, it was deduced that there was tendency to partially recover the nickel anode after exposure to H_2Se, indicating that the adsorption of selenide was temporal and reversible.[30]

Krishnan reported that deposition of significant levels of Hg on electrodes had no degradation effect on the cell components after 150 hours. However, the oxides of mercury however had deleterious effects on the anode by preventing the diffusion and oxidation of H_2 gas leading to reduction in cell efficiency.[31]

Marina et al. and Trembley et al. studied the effect of 0.1-1 ppm of arsines in syngas on Ni/YSZ surfaces and they observed no significant effect in cell output. However, at higher concentrations, Trembley et al. found a decrease in the output of the cell. According to Krishnan, there was a decrease in voltage after 10 hours which later remained constant at 60 hours.[32, 33.]

Krishnan et al. studied the effect of varying operating temperatures on the performance of cell in the presence of antimony oxide. It was observed that at higher temperatures (800 - 850 ºC), the electrodes are degraded in the presence of antimony oxide, leading to a decrease in the output of the cell. For cadmium, research conducted by Krishnan et al. showed that the degradation of the components of the SOFC occurred at elevated temperatures after 70 hours.[31]

According to Ray and Maskalick, zinc did not appear to affect the cell performance during the entire analysis. However, Krishnan et al. observed a slight decrease in cell output at 800 ºC for an analysis period of 120 hours.[34]

CARBON DEPOSITION ON THE SURFACE OF NICKEL ELECTRODES

The fuels used in the SOFC are made of higher percentage of hydrocarbons, which tend to deposit carbon on the surface of nickel electrode. The amount of carbon deposits is influenced by factors such as temperature, pressure, type of anode materials, and the concentration or ratio of the reagents. According to Li, there are three ways by which carbon deposits are formed in the SOFC, which are illustrated below. [35]

a. Low carbon to steam ratio and elevated temperatures, also termed as cracking of methane.

$$\mathbf{CH_4 \rightarrow C + 2H_2} \qquad \mathbf{\Delta H = +75\ KJ/mol}$$

b. Elevated concentrations of CO (referred as the Boudouard equation)

$2CO \rightarrow C + CO_2$ $\Delta H = -172$ KJ/mol

c. Reduction of CO

$CO + H_2 \rightarrow C + H_2O$ $\Delta H = -131$ KJ/mol

Studies conducted by Wei et al. 2020, showed that the carbon deposits on the surface of nickel electrode was affected by the grain size of nickel particles (13.2 -25.4 nm) which eventually led to the deactivation of nickel. [36] Density functional theory (DFT) calculations by Watanabe and Ogura, 2022, showed that the vacancies in configuration at the interface of 8 % Ni/YSZ cermet influenced the formation of carbon on the surface of the anode.[37]

Li explained that there are various species of carbon that are formed on the surface of nickel electrode. The alpha and gamma carbon species are generated at temperatures between 150 - 400 ˚C are usually deposited in the form of carbides on the surface or bulk of the electrode. The formation of the carbide causes irreversible damages to the anode. The polymeric or amorphous carbon films are formed at temperatures of 250 - 500 ˚C and are termed as beta carbon. These amorphous carbon deposits develop into the filamentous carbon species over time. [35]Vermicular filaments or whisker carbon deposits are another form of gamma carbon produced at elevated temperatures (300 -1000 ˚C). They form hardened substances on the surface of the anode and eventually create cracks on the anode. The epsilon carbon species are made of graphite, carbon flakes and carbon nanofibers. They are formed at elevated temperatures usually above 550 ˚C and have the potential to encapsulate the nickel electrode therefore deactivating it. [34] Graphitic carbon is the most stable form of the carbon deposited on the electrodes and its quite difficult to reverse it

once they are formed. It has the tendency to move into the crystal structure of the nickel electrode leading to total disintegration of the anode material.

According to Lee et al. the carbon deposits tend to cover up the three-phase boundary layer and decrease the cell performance by simply blocking the pores of the nickel electrodes. [38] Boldrin et al. explained that by covering the entire monolayer sites of nickel, there is a drastic decrease in the flow of the gases for redox mechanism. [39] Argyle and Bartholomew reported that carbon deposits encapsulate the nickel electrode leading to decrease in accessibility and diffusion of gases. Moreover, excessive deposits of carbon by adsorption leads to formation of cracks and microstructural deformation.[40]

In attempt to mitigate the amount of carbon deposits on the nickel electrode, scientist have developed new anode materials that involve the use of cerium oxides. Cerium has the tendency to widen the TPB and increase the amount of oxide ions available for the oxidation of carbon. The alloys of nickel such as addition of molybdenum, iron, copper and cobalt reduced the amount of carbon deposits.[41]

Another method to control carbon deposits, steam or internal reforming of the hydrocarbons is a cheaper alternative to convert the hydrocarbon fuels completely into carbon dioxide but its dependent on provision of the stoichiometric ratio of the water needed for the reforming process. The short comings of this approach however will be that the excessive amount of water dilutes the fuel and cause a decrease in cell voltage. [42]In 2022, Vafaeenezhad et al. reported that the presence of moisture causes nickel to dissolve and re-deposit on the anode, leading to loss of structural integrity and decrease in potential of the cell.[24]

ELECTROLYTE DEGRADATION

Butz et al. and Hattori et al. described phase transition as a phenomenon in which an electrolyte changes its structure from one to another. At temperatures of about 800 - 1000 ℃ over several hours of operation of SOFCs, the electrolyte undergoes a change from the most stable cubic to the tetragonal structure which destabilizes the chemical structure and lowers the ionic conductivities, performance and durability of the cell. The rate of electrolyte degradation is dependent on the temperature, period, quantity of impurities. [43,44]

REASONS FOR DECREASE IN CELL POTENTIAL

There are numerous reasons that account for the decrease in potential output of the cell namely ohmic, concentration and activation polarization. According to Zalko and Laszlo 2020, polarization is defined as the attraction of electroactive reagents at the surface of the electrodes creating a change in the electrode potentials.[45] There are three types of polarization and these are shown in Fig 1.2.

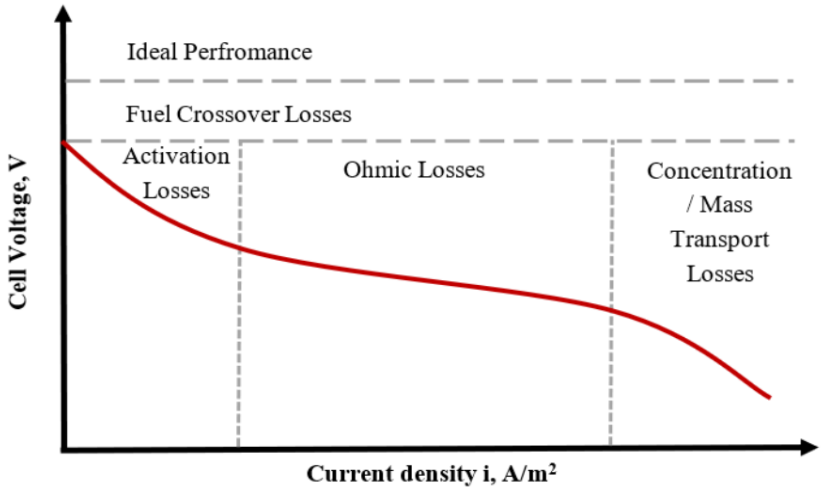

Fig1.2: Polarization of SOFC

http://dx.doi.org/10.1016/j.ijhydene.2013.09.051

OHMIC POLARIZATION

Ohmic polarization is the resistance to the flow of ions in the YSZ. Kikuchi, et al. 2007, explained that the impedances to ionic or electronic flow is mainly attributed to the loss of connectivity between the grains in the nickel anode, reactions between different phases creating a non-conductive layer, resistance created between contact mesh and cell, and finally a decrease in the length of TPB layer. [46] Ohmic resistance is usually the largest due to high resistance of the YSZ electrolyte.[47]

The ionic conductivity of the YSZ electrolyte is a function of temperature and has an inverse relationship between the conductivity and the operation temperature as shown by the equations below.

$$R_I = \text{Ƨ}/\sigma \quad \text{and} \quad \sigma = \sigma_o e^{-E/RT}$$

Where R_I = Ionic resistance, Ƨ= thickness of the YSZ electrolyte σ = conductivity of YSZ electrolyte.

CONCENTRATION POLARIZATION

This occurs because of the changes in concentration of reactants (gaseous species) at the bulk, surface of the electrode and TPB layer. [48]The mass transfer of the gases from the bulk to the surface is mainly diffusion controlled. The porosity of the electrodes plays a vital role in ensuring the diffusion of gases. [47] When the reactants are consumed at a faster rate at the electrode than are transported to it, as happens in Nernstian or reversible reactions, it results in the drop of the potential of the cell due to decrease in faradaic process. For reversible electrochemical cells as in SOFCs, the Nernst equation is given by:

$$E = E^O + RT/n\,F \ln [C_O/C_R]$$

Also, $\eta_{CONC} = RT/nF\ 1n\ (1-I/I_L)$ $I = nFD\ (C_B-C_S)/\delta$ $I_L = nFD\ C_B/\ \delta$

R= universal gas constant

D= Diffusion coefficient

δ = diffusion boundary layer

C_B and Cs are concentrations of reagents at the bulk and surface of electrode.

I_L is the limiting current.

ACTIVATION POLARIZATION

Activation polarization occurs because of accumulation of gaseous ionic species at the interface between the bulk and electrode surfaces which serves as a barrier and tends to impede the transport of air and fuel.[49] This creates a slower reaction by increasing the activation energy of the reactants. The higher the activation energy, the lower the rate of electrochemical reaction. This will eventually cause a reduction in the cell efficiency.

$$\eta act = RT/\alpha nF \ln I/I_O$$

α = electron transfer coefficient

I_O = exchange current density

Kopeliovich 2023, explained that activation potential occurring at the at surface of the cathode produces hydrogen gas bubbles as demonstrated by the following reactions. [50]

Reduction of H^+ to atomic hydrogen

$$H^+ + e \rightarrow H$$

Formation and evolution of molecular Hydrogen

$$2H \rightarrow H_2$$

Eventually, the accumulation of hydrogen bubbles at the cathode creates a barrier and increases the activated complex and retards the chemical reactions. The reagents will take a longer time to get to the cathode hence a drop in the potential.

ADSORPTION ISOTHERMS

Adsorption is a process by which a substance (adsorbate) is attached to the surface of an adsorbent, by physical or chemical means. The amount of adsorbate adhering on the surface of an adsorbent is dependent on factors such as surface area, pressure, temperature, pH and the chemical composition of the adsorbate.[45] There are three models that are used to describe the principles behind the adsorption process in electroanalytical chemistry namely Langmuir, Frumkin and Temkin isotherms.

An electrocatalyst such as nickel is characterized by the presence of active sites where hydrogen gas binds and allows electrochemical reactions to proceed. At the nickel anode, when the hydrogen gas is adsorbed, it gets dissociated from molecular to atomic hydrogen, and then chemically combines with oxygen ions from YSZ to create water and oxygen vacancy or electron deficient oxygen species.[24] The series of chemical conversions is shown below:

ADSORPTION STAGE (ANODE)

$$H_2\,(g) \rightarrow H_2\,(ads)$$

DISSOCIATION STAGE

$$H_2\,(ads) \rightarrow 2H\,(ads)$$

ELCTROCHEMICAL REACTION AT TPB

$$2H(ads) + O^{-2} \rightarrow H_2O + 2e + VO^{\cdot}$$

Langmuir Isotherm

Kalam et al. 2021, mentioned that the Langmuir isotherm has the following characteristics: The adsorbate and adsorbent are homogeneous, the active sites are all equal, at equilibrium, the rates of adsorption and desorption are equal, and finally, there is

no interaction between adsorbates on active sites which leads to solely a monolayer adsorption process. [51] Mathematically, the Langmuir isotherm can be expressed as:

$$q_e = q_o K_L C_e / 1+K_L C_e$$

qo = maximum number of adsorbed species, K_L= Langmuir constant

$$C_e/q_e = 1/K_L q_o + Ce /q_o$$

Thermodynamically, the number of sites occupied by the adsorbate can be calculated from the equation below:

$$S + A \rightarrow SA$$

At equilibrium, $$K = [SA] / [S] [A]$$

[A] is directly proportional to the pressure (P).

Let Θ = number of occupied sites, hence $K = \Theta / (1- \Theta) P$

S= Vacant sites A= Adsorbate SA= surface occupied

Frumkin Isotherm

The Frumkin isotherm exhibits the following features: The adsorbate and adsorbent are heterogenous, and there is an electrostatic interaction between other adsorbates on the active sites of the electrode creating a multilayer adsorption.[52] Frumkin isotherm can be represented by the equation below.

$$C= 1/b \Theta / (1- \Theta) \exp 2w \Theta/RT$$

C= bulk concentration, Θ = fractional loading, b and w are constants, q = amount adsorbed

q_m = specific saturation capacity

$$\Theta = q/q_m$$

$$\ln [\Theta/ (1- \Theta) C] = \ln b – 2w/RT \Theta$$

$$\ln [\Theta/ (1- \Theta) C] = \ln b – 2w/RT\ q/q_m$$

Temkin isotherm

According to Ramanathan, active sites on the adsorbent with more favorable energy are occupied earlier followed by those with less energy. In Temkin isotherm, adsorbates of very low or high concentrations are eliminated. It has similar characteristics as the Frumkin's model.[48]

$$\mathbf{Q_e = RT/b \ ln \ C_e + RT/b \ ln \ K_m}$$

B= Temkin's constant or sorption heat in J/mol

K_m= Temkin isotherm constant

LANDFILL

Landfills are biodegradable and non-biodegradable waste collected and covered up over a period. As water infiltrates through the landfills, micro-organisms convert solid waste into leachate and land fill gases. Landfill gas is collected from underground wells through pipes, processed, flared and treated. It is then used as a fuel to generate electricity.[53] Leachate may contain harmful substances depending on the composition of the waste and end up polluting the environment. To prevent migration of leachates, bioreactors are designed to contain the waste and prevent pollution caused by leachate from the landfills. There are three (3) types of bioreactors which are aerobic, anaerobic and semi aerobic(hybrid).

The aerobic bioreactor allows air and moisture to enter the landfill so that the aerobic bacteria convert waste substances into mainly carbon dioxide. Leachates generated are collected in well-designed systems for future analysis and disposal. This bioreactor system has less greenhouse gas emissions and no pollution from leachates. On the other hand, anaerobic bioreactors systems lack oxygen hence bacteria transform waste into carbon dioxide and methane. These gases are captured and stored as fuels. The hybrid bioreactor systems combine both the aerobic and anaerobic components hence generate about 45 - 60 % of methane, 40 - 60 % carbon dioxide and 2 % of gases made up of water vapor, ammonia, hydrogen sulfides, trace metals, oxygen, siloxanes, aromatics, unsaturated hydrocarbons, and carbonyl compounds. [54, 55]

The composition of the gas generated from landfill gases is dependent on the following conditions:

Age of the landfill- landfills which are less than ten years old will generate higher concentrations of methane and carbon dioxide gases than older landfills. This is solely because bacteria have enough waste to decompose hence generate more LFG.

The type of waste available- bacteria can consume biodegradable waste at a faster rate by breaking down complex chain carbohydrates, proteins and fats into smaller compounds generating carbon dioxide, ammonia and hydrogen sulfides in greater quantities.

Temperature of the environment: In colder temperatures, microorganisms are inactive, and this condition slows down the biodegradation process hence lower emissions of landfill gases. Contrarily, when the temperature rises, activity of microbes escalates, and this generates higher concentrations of LFG.

Presence of moisture and oxygen: Elevated levels of water and oxygen promote the growth and multiplication of microorganisms hence the conversion of waste to leachate and LFG increases.

CHAPTER TWO

INSTRUMENTATION, METHODOLOGY AND EXPERIMENTAL WORK

PREPARATION OF COATED YSZ ELECTROLYTE

Liquid Bright Platinum, lanthanum strontium manganite (LSM) and yttria-stabilized zirconia (YSZ-8) substrate button cells of diameter 20 mm, and thickness of 0.26 mm were purchased from Fuel Cell Materials-Nexceris and Heraeus. The YSZ-8 button were coated with platinum, nickel-YSZ with 1% binder as well as LSM/YSZ ink, air dried for about 30 minutes and heated in an oven for four hours at 1000 ˚C at a heating rate of 300 ºC/hr for a period of 6-8 hours. This procedure causes sintering which improves the mechanical stability and ionic conductivity of the electrodes.

Pre-analysis of uncoated YSZ substrate which acted as a control, then the nickel/YSZ with 1% binder, LSM/YSZ and platinum coated YSZ substrates were performed using XRD, Scanning Electron Microscopy and Energy Dispersive Spectroscopy (SEM-EDS) as shown in Fig 2.1 and Fig 2.2 respectively. The pre-analysis stage was important since it provides information on the atomic and weight percentages of elements on the substrates prior to analysis and after the deposition of carbon during the passage of methane and propane gases. It also a way to confirm the composition of the substrates as indicated on the MSDS of the manufacturer. The substrates were mounted on the plates using carbon and copper supports. They were then placed in the SEM-EDS machine. Magnifications and focal points were adjusted and an image of the YSZ substrates were obtained as well as the EDS data. [17,18]

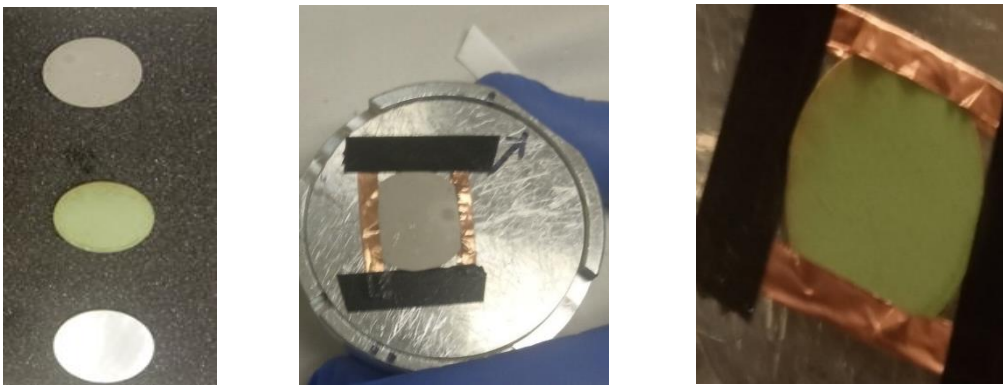

Fig 2.1: Images of YSZ substrates

The substrates were placed on the sample holder of the Bruker XRD instrument and the d-spacing was obtained. The results for the d-spacing were compared with the built-in library for the compounds which gave information on which compounds exactly matched up with the sample. This helped in identifying the composition of the compound.

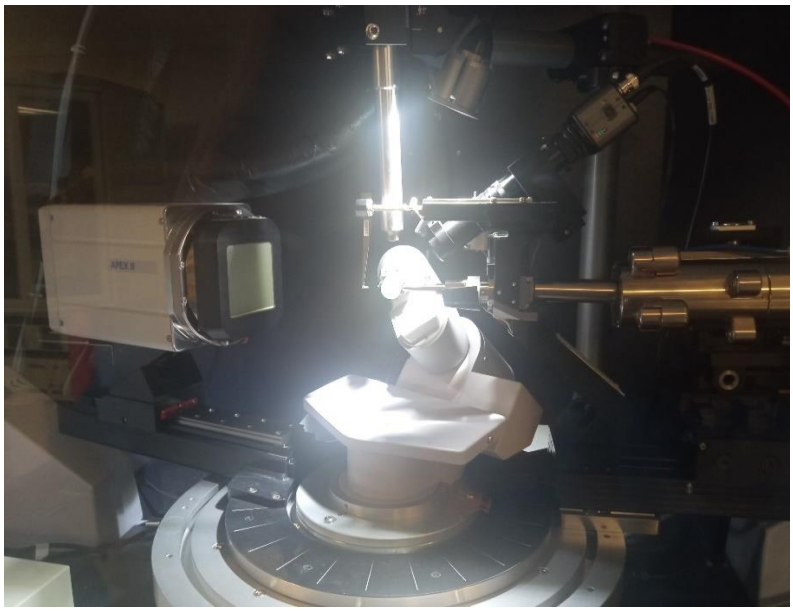

Fig 2.2: XRD analysis of Pt/YSZ/Pt cell

PROBOSTAT™

The Probostat™ is a device used for electrochemical measurements at elevated temperatures between 750 -1200 ºC, determines the electrical properties and aids in the characterization of materials, and studies the rate of exchange of gases at the surface of electrodes in a fuel cell. It is made of ceramic material containing alumina or silica as shown in Fig 2.3. The contacts of the SOFC were cleansed in nitric acid and exposed to a hydrogen flame for a few minutes. This procedure was necessary to remove impurities that were deposited on the surface of the contacts. Then, the continuity of the wire was measured using a multimeter. The platinum coated YSZ electrolyte was fixed on the inner tube by using a Ceramabond purchased from Aremco. It was air dried for about one (1) hour. The anode was then fixed at pin number 13 as shown in Fig 2.4 below. This was then supported by three rods connected to `triangular shaped structure and held in place by the springs. The outer cover was placed on it and screwed in place by the metal ring. [17,18]

Fig 2.3: Diagram of Probostat™

Fig 2.4: Position of pins on Probostat^{TM}

The final setup was placed in the fume hood and the temperature was increased to 93 ˚C for two hours and finally 260 ˚C for another two hours to complete the curing process as shown in Fig 2.5 below.

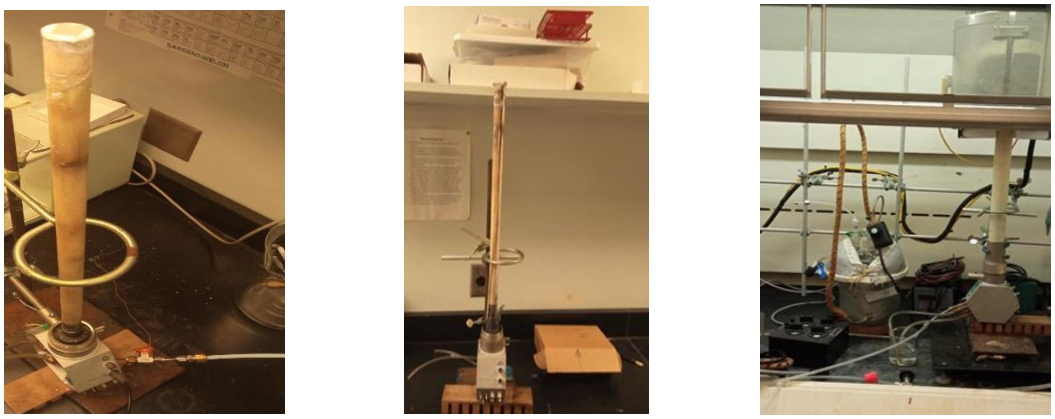

Fig 2.5: Setup for SOFC

GAS STORAGE TANKS AND FLOW METERS

Ultra-High Purity (UHP) propane, methane, hydrogen, argon and compressed air gases were used for the SOFC experiments as can be seen in Fig 2.6. The gas tanks were used to store the fuel and are controlled by valves. There is a pressure valve that helps to regulate the pressure to about 30 psi and there are valves that help in the flow of the gas through the gas tubes. The volume of gas that flows through the tubes is regulated by the gas flow meters and is set to about 50 ml/min as demonstrated in Fig 2.6. The air is made to pass through the cathode compartment whilst the fuels flow through the anode. The anode compartment is usually purged with air or nitrogen gas prior to the passage of the fuel.

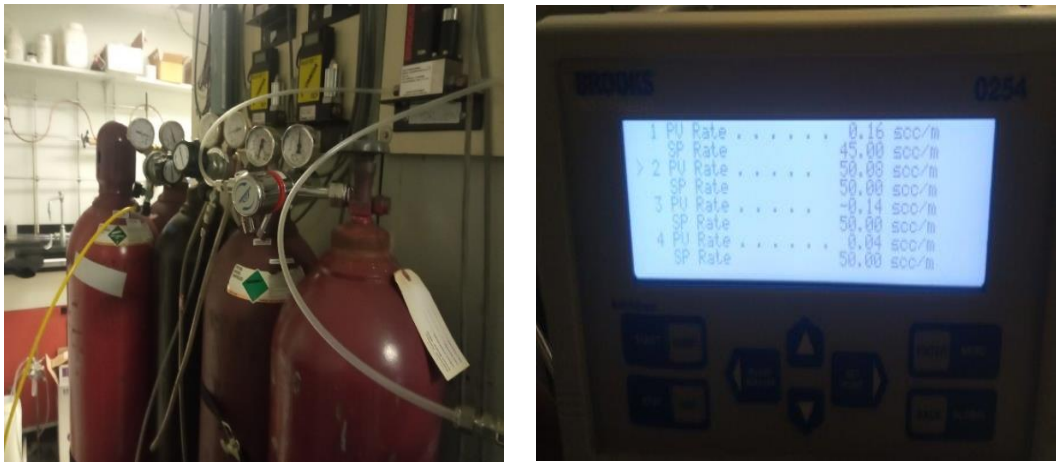

Fig 2.6: Gas storage tanks and gas flow controller

GAS LEAK TESTS

To generate electricity, the fuel is passed through the anode compartment whilst air goes through the cathode compartment. Prior to the passage of the gas, it is imperative to determine whether there is a leakage in the two compartments to avoid explosion. The first procedure was to pass air through the inlet of the cathode and observed whether there was gas flow at the outlet of the cathode but not the anode. Similarly, gas was passed through the anode compartment and the outlet was observed to check for flow of gas. To identify were the was leaking, another test was performed by using soap solution. Soapy solution was placed on the YSZ and the bottom whilst air was passed through the cathode. The presence of bubbles indicated that there was a leak as can be seen in Fig 2.7.

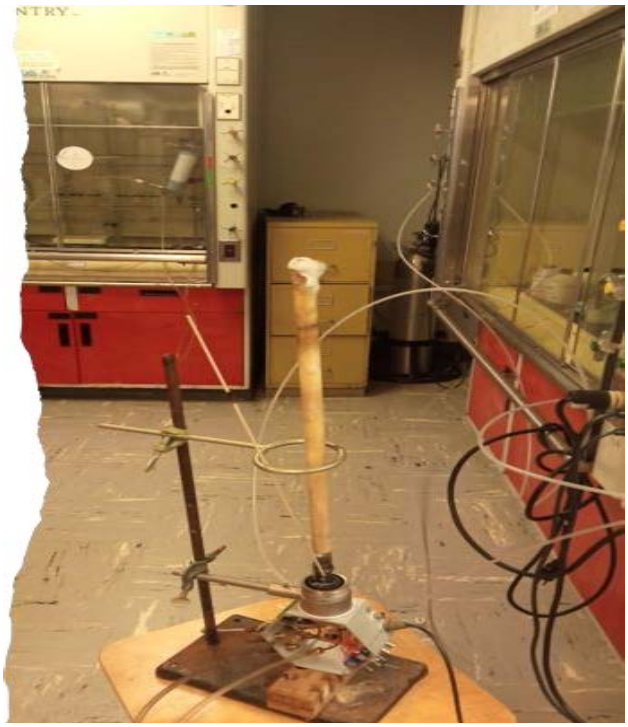

Fig 2.7: Gas leakage test

CURRENT-VOLTAGE MEASUREMENT OF SOFC IN ELECTROLYTIC MODE

Current-voltage measurements were measured at a temperature of 750 ºC, where the resistance of YSZ was lowest. The setup for voltametric readings can be found in Fig 2.8. The ammeter was connected in series and the voltmeter was in parallel with the Probostat^{TM} as seen in Fig 2.10. The power supply was dialed gradually from 0.00 to 1.00 V and the current was obtained at each stopping potential. The voltage was then dialed back from 1.00 to 0.00 V and current was recorded. Voltage-current curves were obtained as shown in Fig 2.8 and Fig 2.9 below.

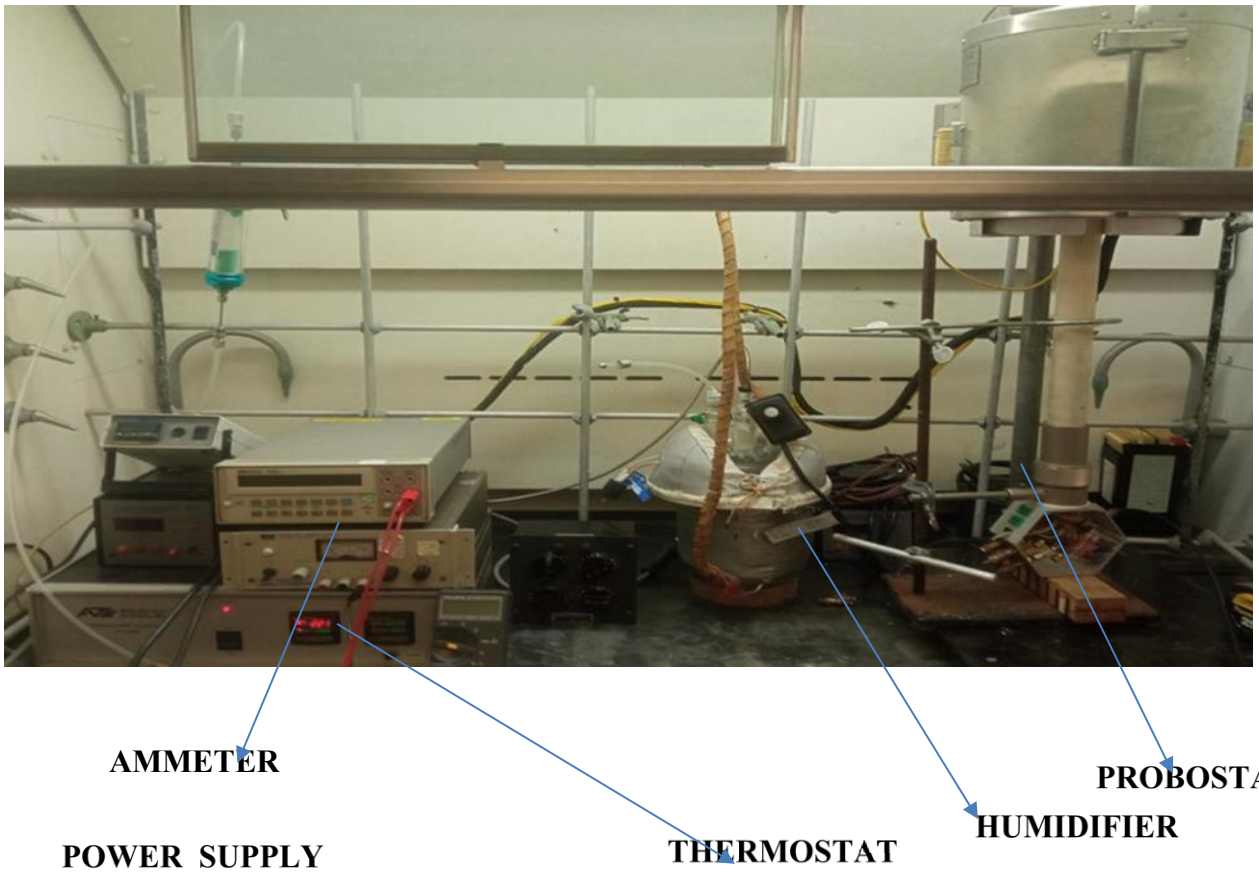

Fig 2.8: Setup for voltammetric readings

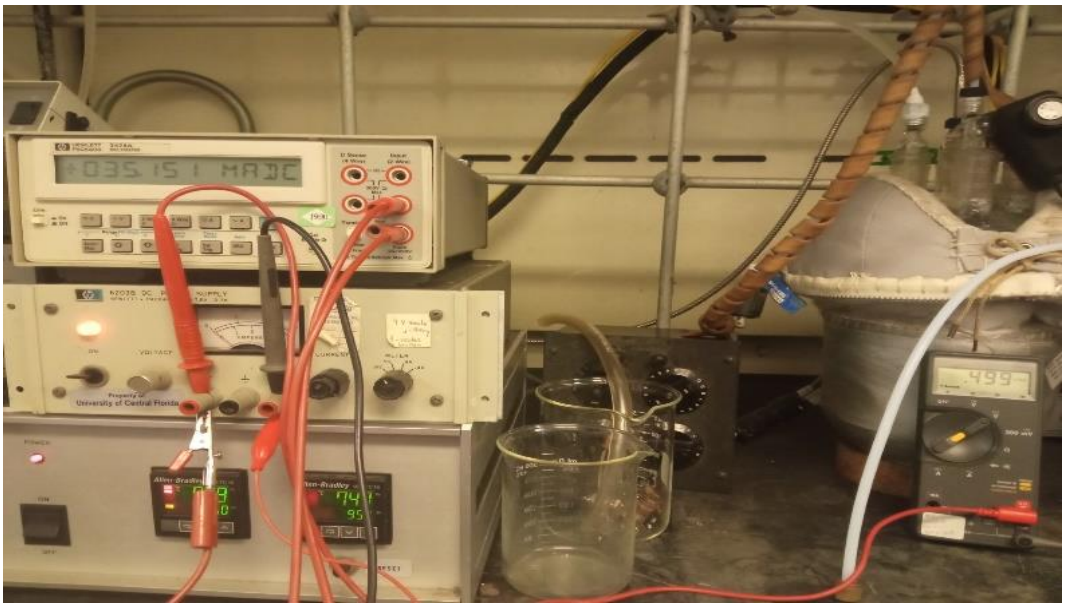

Fig 2.9: Current of $Pt/O_2/YSZ/Pt/O_2$ cell

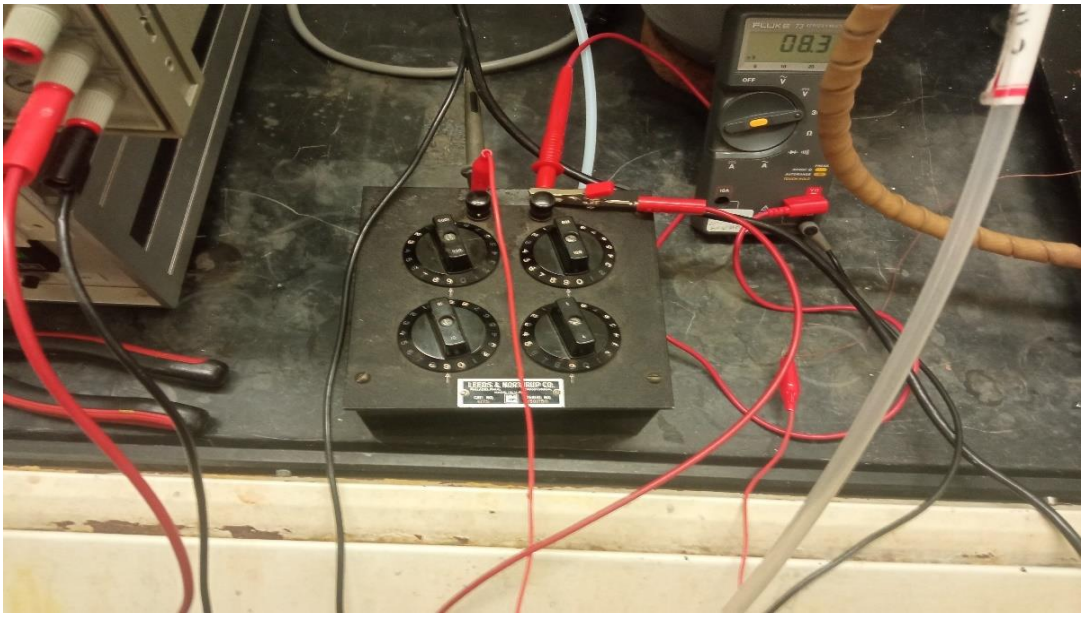

Fig 2.10: Resistor in series with ammeter

CHAPTER THREE

RESULTS AND DISCUSSION

PRE-ANALYSIS OF CONTROL AND COATED YSZ SUBSTRATES USING SEM- EDS AND XRD

It was observed from the data collected as shown in Table 3.1 that there were higher atomic percentages of oxygen in the control YSZ substrates followed by zirconium and yttrium. This is also observed in the spectra for the control YSZ substrate in Fig 3.1. This confirmed that the substrate is primarily made of oxides of yttrium and zirconia. The higher percentage of oxygen and differing valency of host Zr and dopant Y suggests that the substrate is an oxide ion conductor. The results obtained were comparable to the elemental composition provided on the material safety data sheet (MSDS). Control cells also showed the presence of aluminum, hafnium and nickel which were less than 1%. Hafnium and aluminum are added as dopants to improve on the conductivity and stability of YSZ. Aluminum oxides act as sintering agents to densify the electrolyte. Brodnikovska et al. explained that addition of a dopant to YSZ, such as scandium, cerium and yttrium, enhances the flow of ions by increasing oxygen vacancies, and lowers the ohmic resistance.[56]

Table 3.1: Pre-analysis of control YSZ with SEM-EDS

ELEMENT	WEIGHT %	ATOMIC %
O	59.05	88.91
Al	0.35	0.31
Y	6.23	1.71
Zr	34.39	9.07

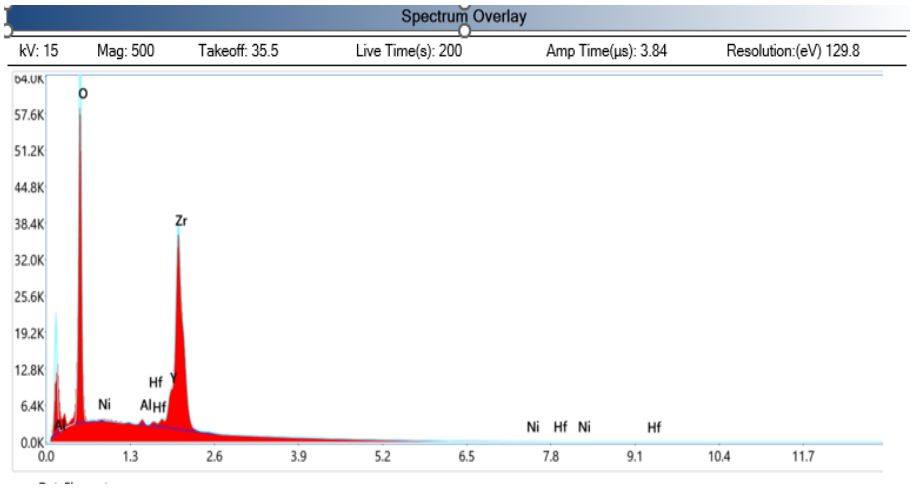

Fig 3.1: Pre-analysis of control YSZ

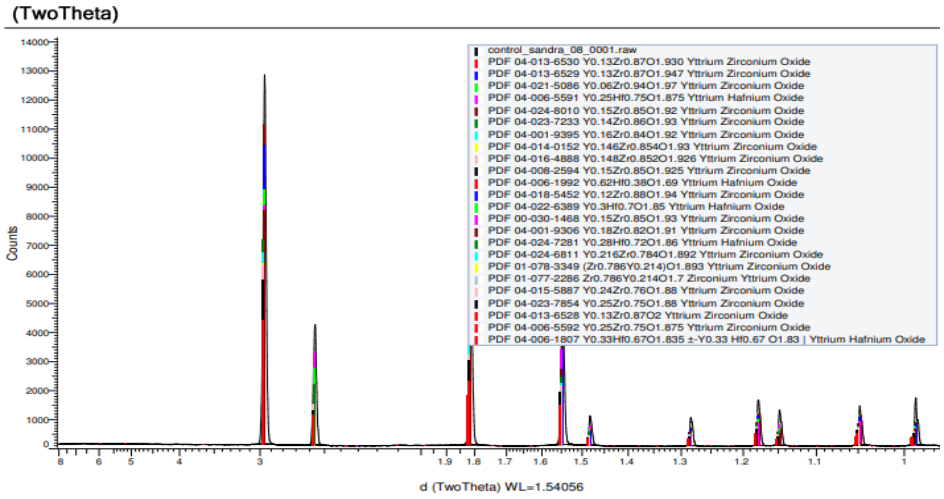

Fig 3.2: XRD analysis of control YSZ

The XRD spectrum shown in Fig 3.2 above is most likely to be $Y_{0.06}\ Zr_{0.94}\ O_{1.97}$.

The upper and lower sections of the YSZ substrates were coated with platinum ink and a pre analysis of the platinum coated yielded a very high percentage weight of platinum as observed in table 3.2 and its spectra in Fig 3.3. The higher atomic weights of carbon could be attributed to volatile organics and aerosols from the atmosphere, as well as the use of carbon tapes for supporting the samples on the plate.

Table 3.2: SEM-EDS analysis of Pt/YSZ/Pt cell

ELEMENT	WEIGHT %	ATOMIC %
C	6.48	41.00
O	4.99	23.70
Pt	88.54	35.30

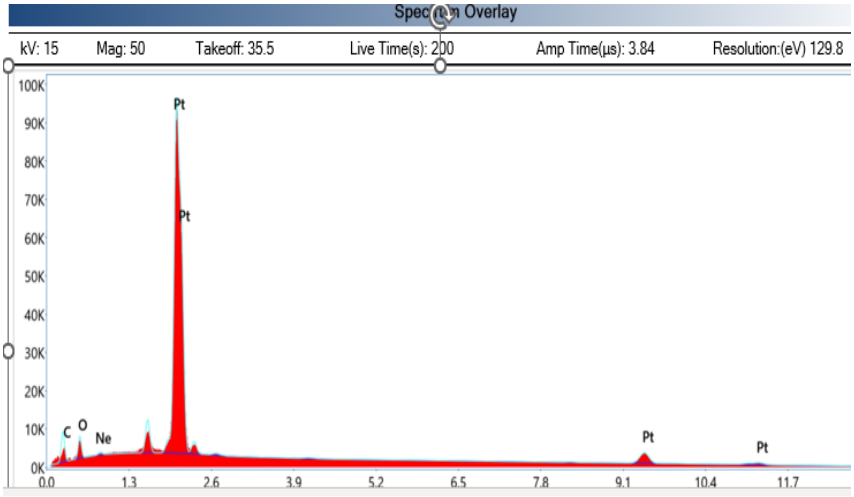

Fig 3.3: Pre-analysis of Pt/YSZ/Pt cell

The XRD spectrum in Fig 3.4 indicates the presence of platinum on the surfaces of the electrode with Platinum Zirconium as the most probable compound.

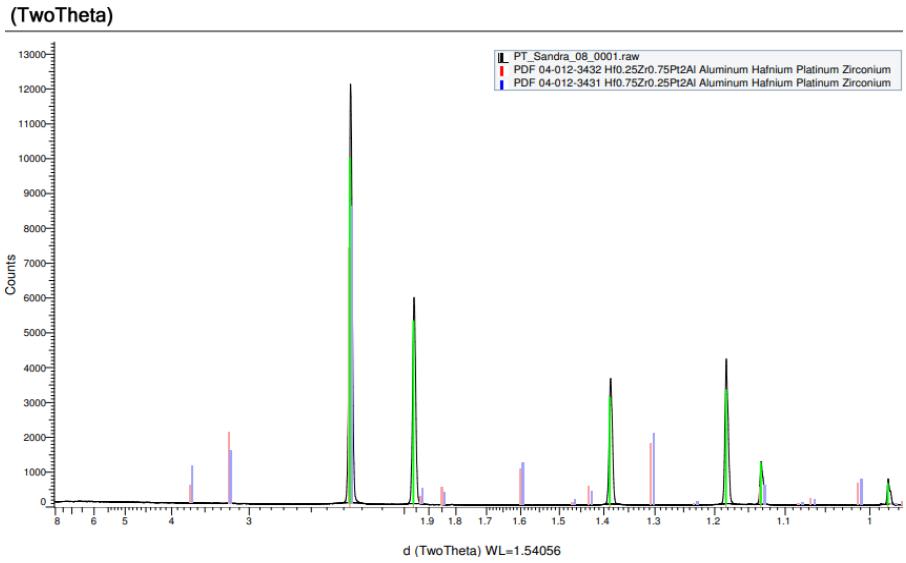

Fig 3.4: XRD analysis of Pt/YSZ/Pt cell

The nickel coated YSZ substrate showed higher percentage of nickel (26 %), whilst there was also a slight increase in the zirconia. However, the percentage weight of oxygen decreased by almost half the original value of the control sample as shown in table 3.3 and Fig 3.5.

Table 3.3: SEM-EDS analysis of Ni/YSZ cell

ELEMENT	WEIGHT %	ATOMIC %
O	29.68	66.78
Ni	26.54	16.35
Y	5.94	2.41
Zr	35.73	13.96
Hf	2.48	0.50

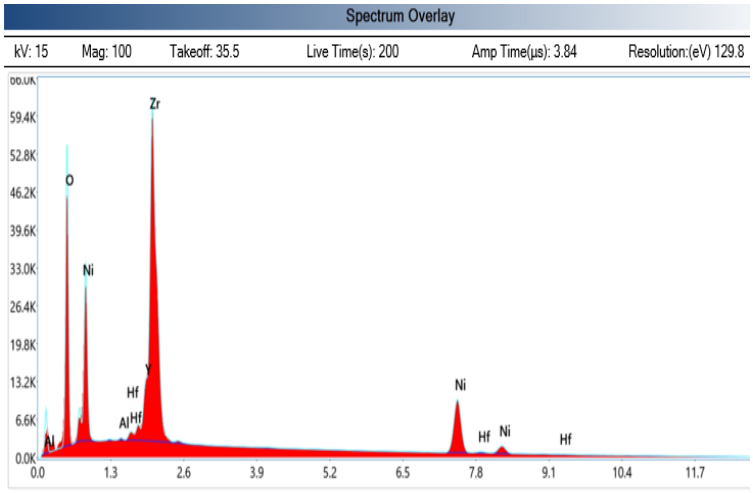

Fig 3.5: Pre-analysis of Ni/YSZ cell

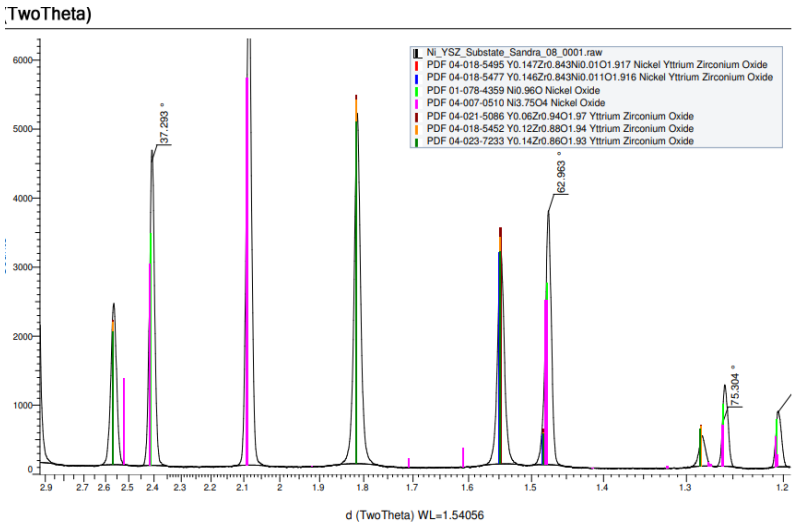

Fig 3.6: XRD analysis of Ni/YSZ cell

From the XRD spectra shown in Fig 3.6, the most probable compound present in the surface of the above substrate is $Y_{0.06}Zr_{0.94}O_{1.97}$.

VOLTAGE-CURRENT MEASUREMENTS OF SOFC IN GALVANIC AND ELECTROLYTIC MODE

The resistance of the $Pt/O_2/YSZ/Pt/O_2$ cell was measured at 750 ºC and 900 ºC. The voltage-time plots were obtained for a period of one (1) hour as it helped to determine if the cell was electrically conductive, and the results are shown in Fig 3.7 below.

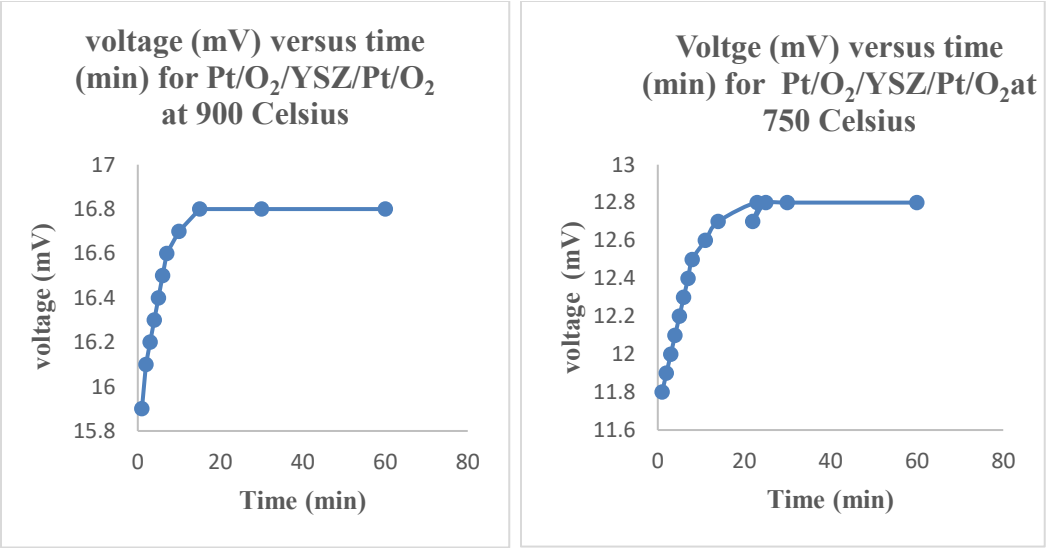

Fig 3.7: Voltage-time plot of $Pt/O_2/YSZ/Pt/O_2$ cell

DEPENDENCE OF RESISTANCE ON TEMPERATURE FOR YSZ

To determine the dependence of temperature on the resistance of YSZ, the Probostat™ was heated from 322 ºC to 750 ºC during the passage of hydrogen gas. The resistance of the cell was overload, which means it was extremely high and the value was usually about 32.46 MΩ. The lowest resistance of 11.1 Ω for the YSZ cell was found at 750 ºC after passing H_2 gas for 41 minutes as can be observed in Fig 3.8. This is attributed to the fact that hydrogen gas abstracts oxide ions from the YSZ leading to the formation of reduced zirconia. Zirconia is an insulator, and one characteristic of an insulator is that they possess a band gap of 5 eV between the valence and conduction band.[57] At room

temperature, the electrons in YSZ occupy the valence band and do not have enough energy to move into the conduction band. At higher temperatures, the electrons in YSZ have excess energy, vibrate and are released into the conduction band, leading to an increase in conductivity. YSZ has its highest conductivity of 0.02 $S \cdot m^{-1}$ – 0.1 $S \cdot m^{-1}$ at 800 -1000 ºC.

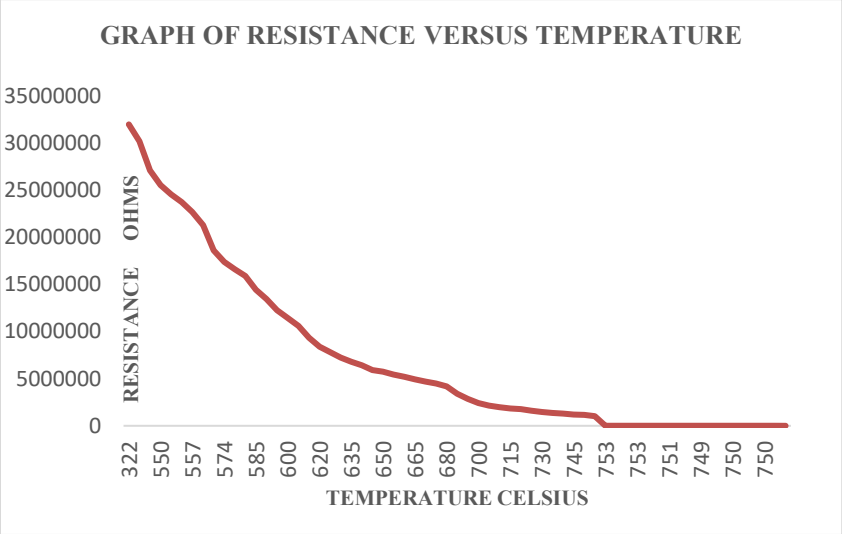

Fig 3.8: Resistance versus temperature

DETERMINATION OF ACTIVATION ENERGY OF ZIRCONIA

Activation energy (E_a) is the minimum amount of energy needed for reactants to go over the transition state to form products. Activation energy of YSZ is temperature dependent, because higher temperatures increase the thermal energy factor, RT, which enables the system to reach the transition state energy. Elevating the temperature creates higher and faster oxide ion conduction in the lattice, to the anode, leading to an overall increase in the rate of the redox reaction. According to Stortelder 2005, activation energies provide information on the availability and mobility of free oxygen vacancies. At low temperatures, activation energy is used to free oxygen vacancies in zirconia whilst at higher temperatures, it enhances the movement of oxygen ions. [58]

From the Arrhenius model, the activation energy is given by $R = Ae^{-Ea/RT}$

Where R= gas constant, T= temperature in Kelvin, R= rate of reaction and A= Arrhenius constant. $\mathbf{\ln R = -E_a /R(1/T) + \ln A}$

The inverse of the resistance was plotted against the inverse of absolute temperature, and straight line is obtained. From the slope of the line, the activation energy of YSZ was calculated as shown in Fig 3.9. The E_a value represents the hopping of lattice oxides (O^{2-}), in the crystal structure of the zirconia.

$$\mathbf{R = \rho\ L/A,\ and\ \rho = 1/\sigma}$$

$$\mathbf{1/R = \sigma\ (A/L)}$$

$$\mathbf{\ln (1/R) = \ln \sigma\ (A/L)}$$

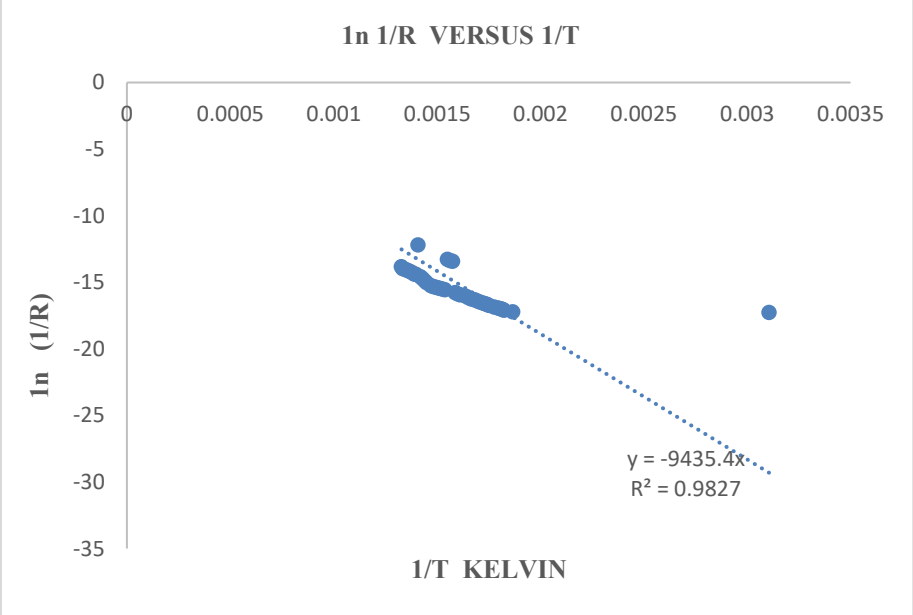

Fig 3.9: Derivation of activation energy for $O^{=}$ transport in ZrO_2

SLOPE = -9435.4 K^{-1} = $-E_a$ /8.314 J/mol·K = 78.9 kJ/mol

The E_a obtained in this experiment was closer to the literature value reported by Stortelder, which was between 0.6 -1.1 eV, and equivalent to 20.7 kcal/mol or 86.53 kJ/mol.[58] Similarly, in 2003, research conducted by Kil et al. on the oxygen diffusion in YSZ, showed that the activation energy of zirconia was between 0.8 -1.0 eV.[59]

SOLID OXIDE ELECTROLYIC CELL

To operate the cell in the electrolytic mode, the negative terminal becomes the cathode whilst the positive terminal is made the anode. This requires a supply of direct current through the cell, hence nonspontaneous. The results obtained for the operation of the platinum coated YSZ substrates and passage of air under electrolytic mode is shown in Fig 3.10 below. By dialing the voltage from 0.00 to 1.00 V and vice versa, it could be proved that in both directions, the data generated from the cell were reproducible. Moreover, the data obtained showed that the electrochemical reaction was reversible. Consequently, the current increased as the voltage increased for both directions and the maximum current generated was found to be 72.6 mA.

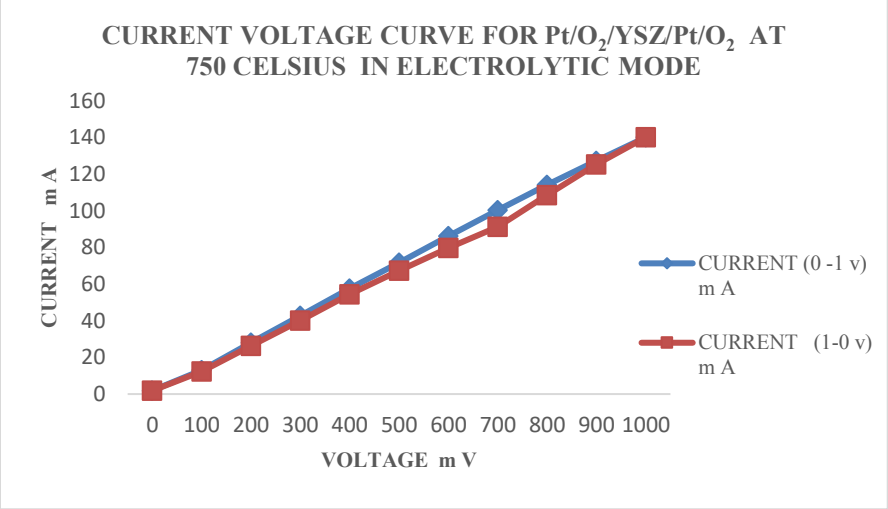

Fig 3.10: Current-voltage plot for $Pt/O_2/YSZ/Pt/O_2$

ELECTROCHEMICAL REVERSIBILITY OF CELL IN ELECTROLYTIC MODE

The current-voltage plots of the electrolytic cell were obtained for dry argon gas and ambient air by dialing the voltage from 0.00 to 1.50 V and then reversing the potential from 1.50 to 0.00 V. As shown in Fig 3.12, the maximum current obtained under dry argon was 156.3 mA.

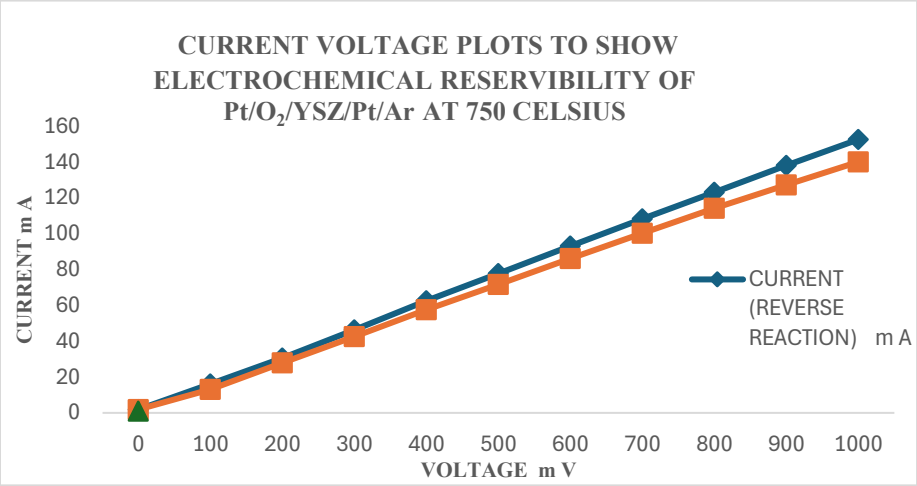

Fig 3.11: Current-voltage curve for $Pt/O_2/YSZ/Pt/Ar$

To analyze the humidified argon gas samples, the temperature controller for the water bath was set to 89.6 ºC, which produces a vapor pressure of 517.88 mm Hg. This value was chosen because 66.67 % of water by volume will be required for the complete reforming of methane as shown in the chemical equation below.

$$\mathbf{CH_4 + 2H_2O \rightarrow CO_2 + 4H_2}$$

The argon gas was passed through the inlet of the humidifier with its outlet connected to the anode of the Probostat^{TM}. The humidifier was covered to prevent heat loss and minimize condensation of water. The corresponding data for the currents achieved are shown in Fig 3.13.

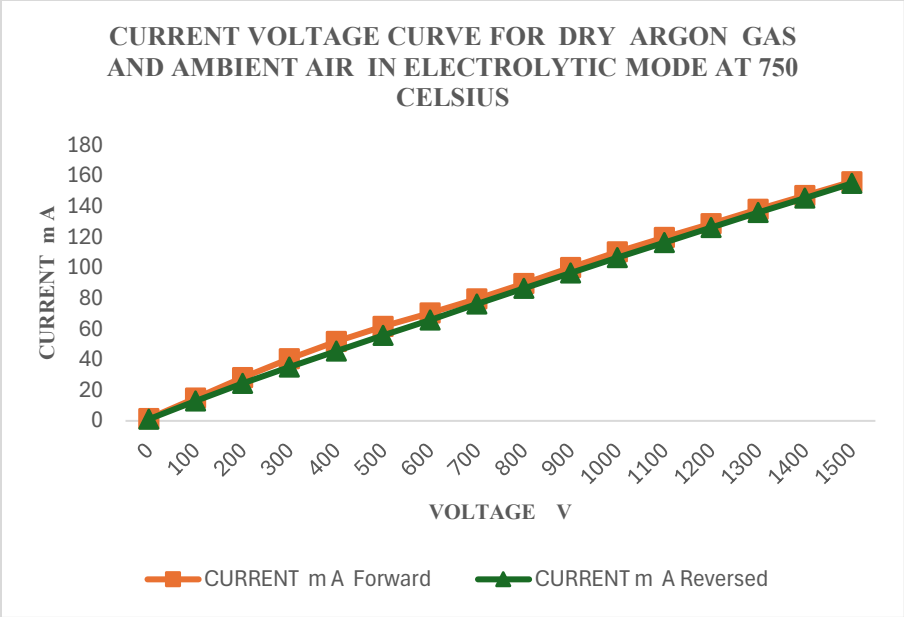

Fig 3.12: Current-voltage plot for Pt/O_2/YSZ/Pt/Ar

In contrast to the dry gas, it was observed that currents in the presence of humidified argon gas at room temperature had lower values, with the maximum around 115.1 mA as seen in Fig 3.13 and Fig 3.14 respectively. This could be attributed to the fact that in the electrolytic mode, the negative terminal serves as cathode and the passage of argon depletes the oxygen content of the TPB, leading to a decrease in conductivity and increase of resistance of the cell. This will eventually lead to a decrease in current of the cell. This could explain why the addition of water had no catalytic effect on the cell. Furthermore, Liu et al. mentioned that the high current generated during the SOEC mode coupled with the decrease in partial pressure of oxygen could potentially lead to increase in polarization resistance.[60]

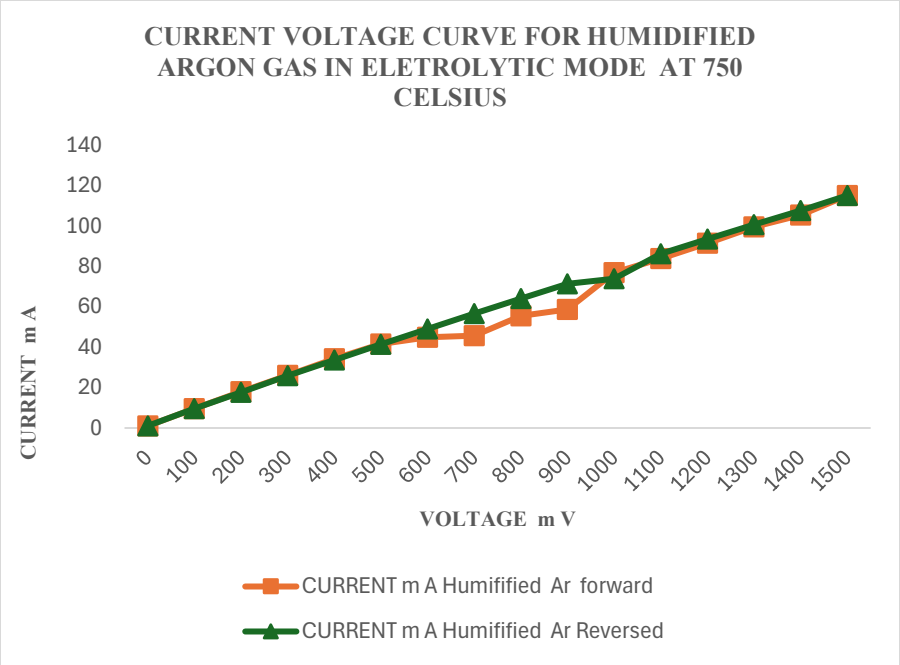

Fig 3.13: Current-voltage plot for Pt/O_2/ YSZ/Pt/Ar.H_2O

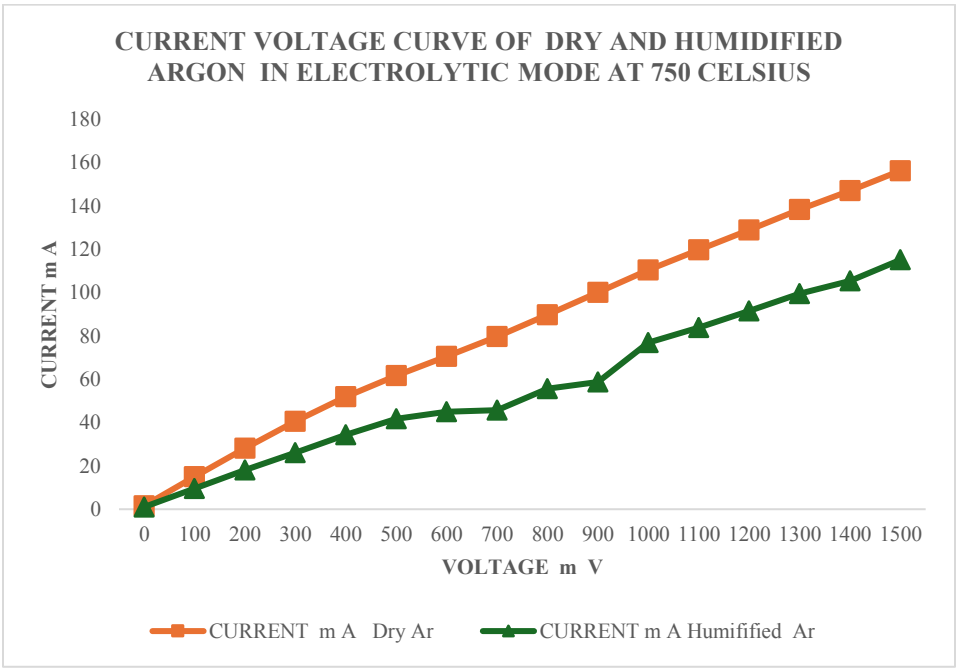

Fig 3.14: Current-voltage curve for Pt/O_2/YSZ/Pt/Ar

After the electrolytic studies, a galvanic cell was made by supplying dry and humidified hydrogen gases to the set-up for 30 minutes, as shown in Fig 3.15. The results obtained were in alignment with the reports made by Wagner et al. that proved that the presence of moisture in the fuel increased the electrochemical performance of the cell.[61] Similarly, in an experiment conducted to study the impact of water on SOFC performance, Montinarro et al. prepared humidified hydrogen gas, composed of 3 % of water to H_2 gas mixture and observed an increase in the voltage of the cell. This is because water vapor has a catalytic effect by lowering the activation overpotential and increasing the oxidation of hydrogen to form water.[62]

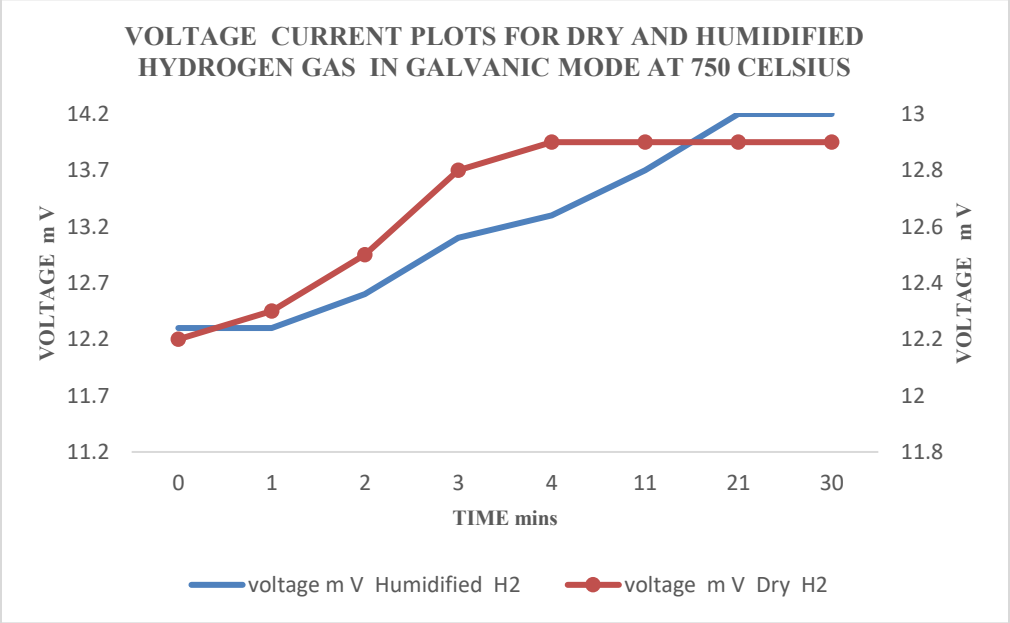

Fig 3.15: Current-voltage curve for $Pt/O_2/YSZ/Pt/H_2$

POST- ANALYSIS OF Pt/ YSZ/Pt CELL AFTER HUMIDIFICATION USING SEM- EDS

The Pt cell was found to be cracked after the humidification process, and this was likely to be attributed to the high current densities, sintering of the platinum atoms at high temperatures and the high flow rates (75 ml/min) of the gases, which might have exerted so much vapor pressure on the system. However, the results from the elemental analysis of the Pt/YSZ/Pt substrates showed no significant changes in composition to the results obtained from the pre analysis using SEM-EDS as shown in table 3.4 and Fig 3.16.

Table 3.4: Post-analysis of Pt/YSZ/Pt cell by SEM-EDS

ELEMENT	WEIGHT %	ATOMIC %
C	6.48	41.00
O	4.99	23.70
Pt	88.54	35.30

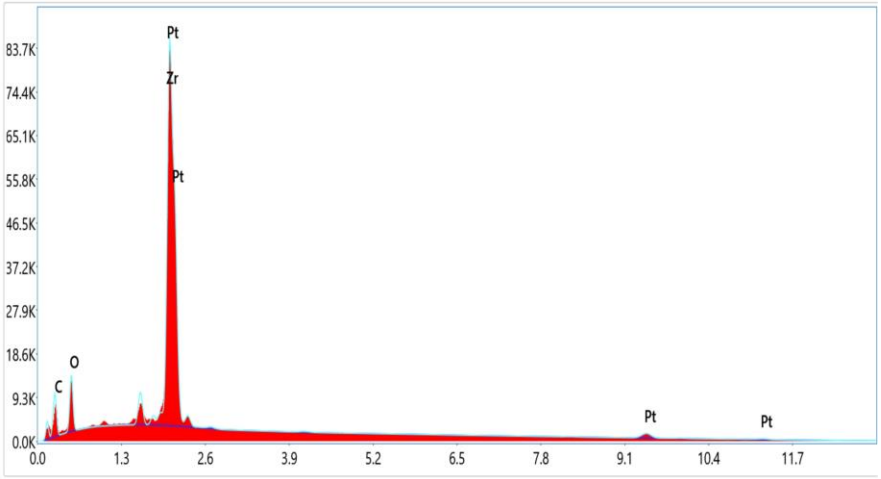

Fig 3.16: Post-analysis of Pt/YSZ/Pt cell by SEM-EDS

EFFECT OF NICKEL CATALYST ON HYDROGENATION REACTION

There are several catalysts used in SOFC, such as platinum, ruthenium, nickel and palladium. Transition metal catalysts have empty d-orbitals that make them reactive to methanation, reforming, and cracking of C-C bonds. In hydrogenation reactions, nickel catalyst and works by adsorbing the hydrogen gas, dissociates it into atomic form, which allows it to bind easily with O^{-2} from YSZ lattice.[63] The nickel first binds with lattice oxides to form NiO, which possess surface oxygens that are reactive and so facilitates the transfer of oxide ion to the atomic hydrogen and eventually form water. Sometimes, if NiO is used as the anode material, hydrogen is passed through the cell to reduce it to nickel, which has higher surface area, extremely active and can exhibit its full potential as a catalyst.[64] Ni catalyst works excellently at the operating temperature of SOFC whilst Pt works efficiently at room temperatures. In comparison with Ni, Pt may not be a good catalyst during reactions with water. This accounts for the catalytic activity of Pt over Ni as shown in Fig 3.17.

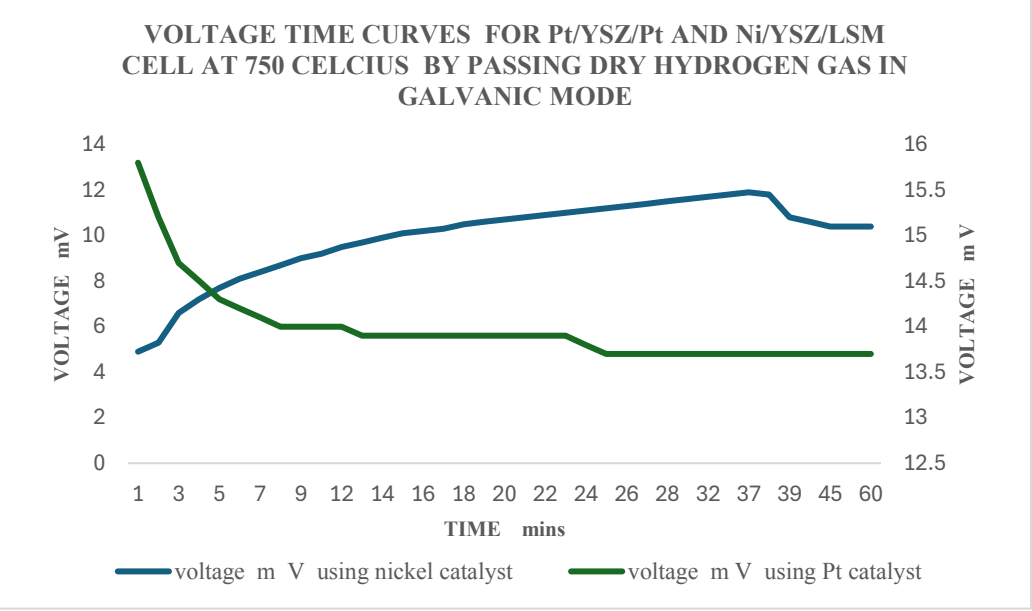

Fig 3.17: Voltage-time plots for Ni and Pt

VOLTAGE-CURRENT CURVES FOR HUMIDIFIED HYDROGEN, METHANE AND PROPANE AT 750 ^{o}C USING Ni/YSZ/LSM

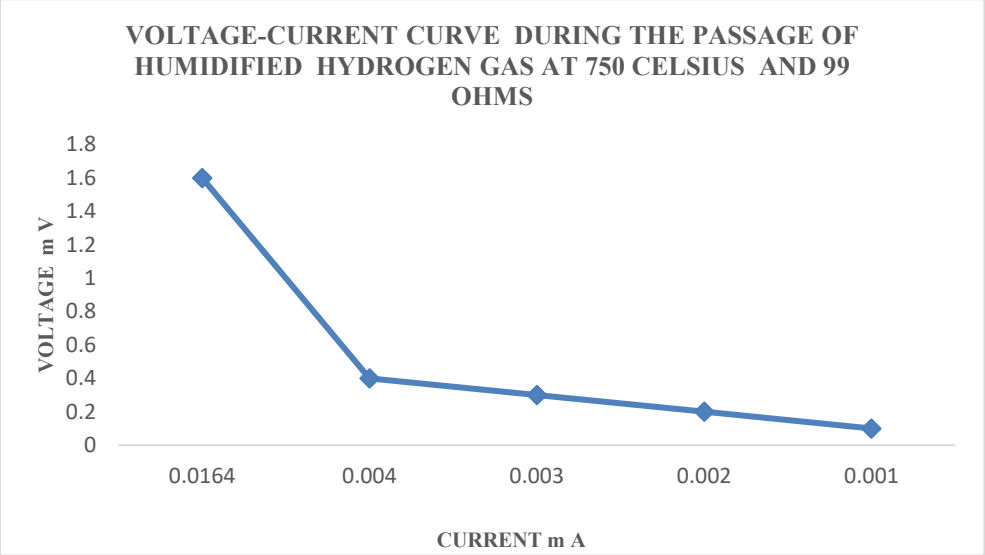

Fig 3.18: Current-voltage plot for humidified H_2 gas at 99 Ω

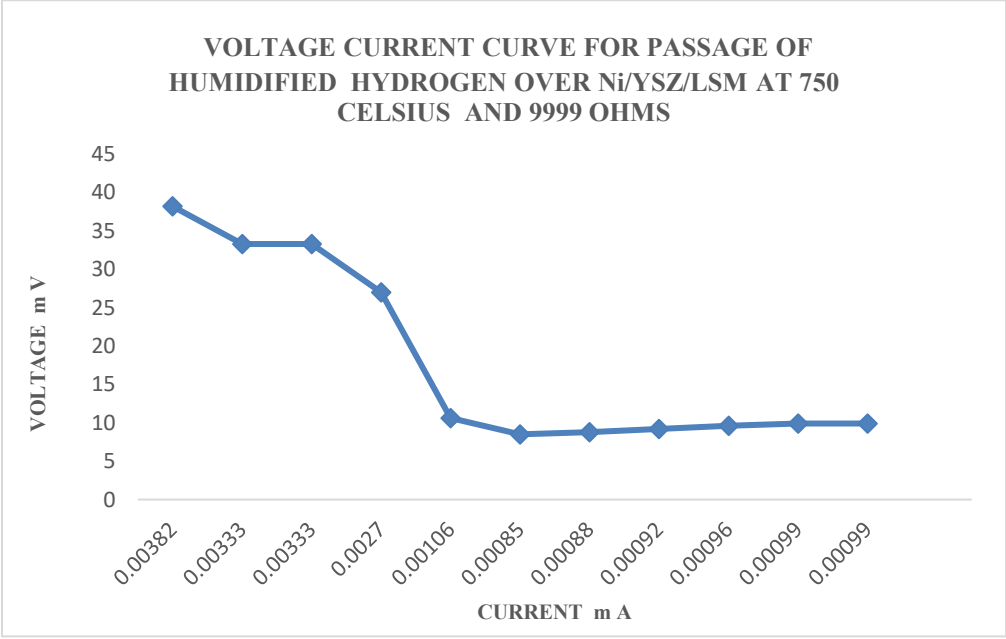

Fig 3.19: Current-voltage plot for humidified H_2 at 9999 Ω

The analysis of humidified methane at 9999 Ω and 99 Ω produced higher currents in comparison to the humidified hydrogen under the same conditions as can be observed in Figs 3.18, 3.19.3.20 and 3.21 respectively. This could be related to the fact that the humidified methane generates 4 moles of hydrogen gas by the steam reforming process. The hydrogen gas serves as the main fuel for the SOFC, thereby creating a greater cell performance as shown in the chemical equations below

Humidified Hydrogen

$$2H^{+} + O^{-2} \rightarrow H_2O$$

Humidified methane – steam reforming

$$CH_4 + H_2O \rightarrow CO + 3H_2 \qquad \Delta H = +206\ KJ/mol$$

Water gas shift

$$CO + H_2O \rightarrow CO_2 + H_2 \qquad \Delta H = -41\ KJ/mol$$

$$CH_4 + 2H_2O \rightarrow CO_2 + 4H_2 \qquad \Delta H = +165\ KJ/mol$$

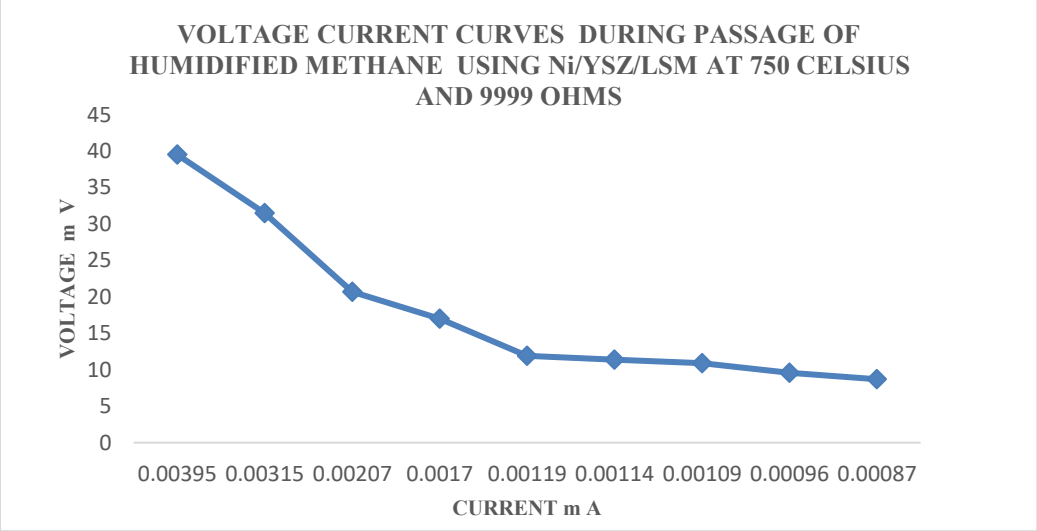

Fig 3.20: Current-voltage curve for humidified CH_4 at 9999 Ω

In Fig 3.21, it can be observed that a higher current ranging from 0.089 - 0.007 mA was obtained when humidified methane gas was passed through the Ni/YSZ/LSM cell button operated at a resistance of 99 Ω**.** Conversely, the current generated at 9999 Ω ranged from 0.004 - 0.0009 mA as shown in Fig 3.20. There was an inverse relationship between the voltage and current generated from the cell.

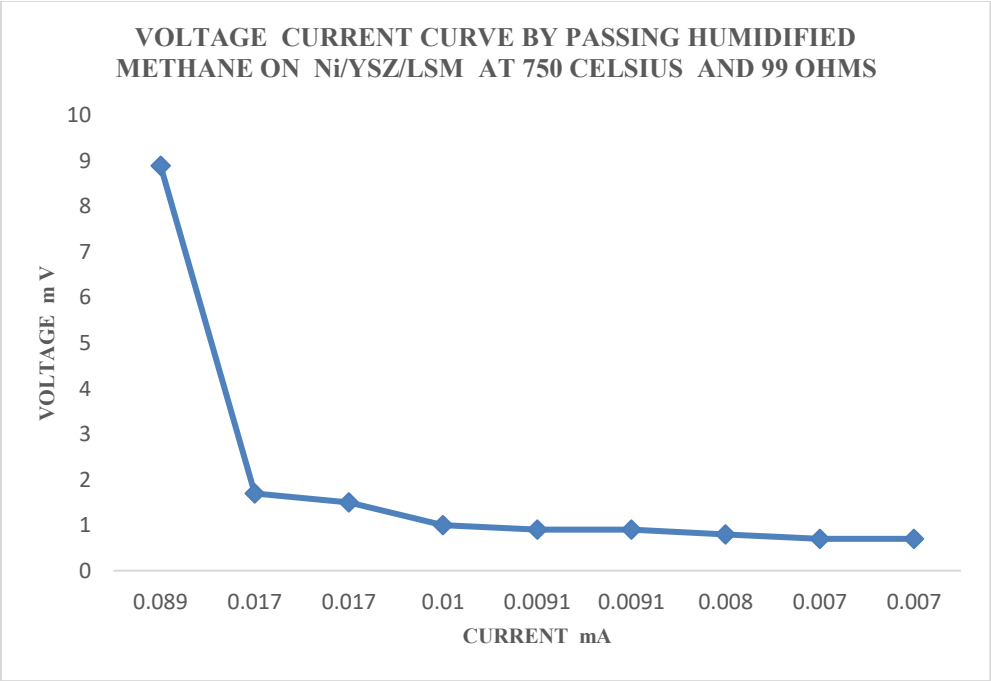

Fig 3.21: Current-voltage curve humidified CH_4 at 99 Ω

In Fig 3.22, a similar trend in cell performance was observed when the gas was changed from methane to propane. The propane gas generated 10 moles of hydrogen gas which makes it a better fuel by enhancing the voltage and current outputs.

$C_3H_8 + 3H_2O \rightarrow 3CO + 7\ H_2$

$3CO + 3H_2O \rightarrow 3CO_2 + 3H_2$

$C_3H_8 + 6H_2O \rightarrow 3CO_2 + 10\ H_2$

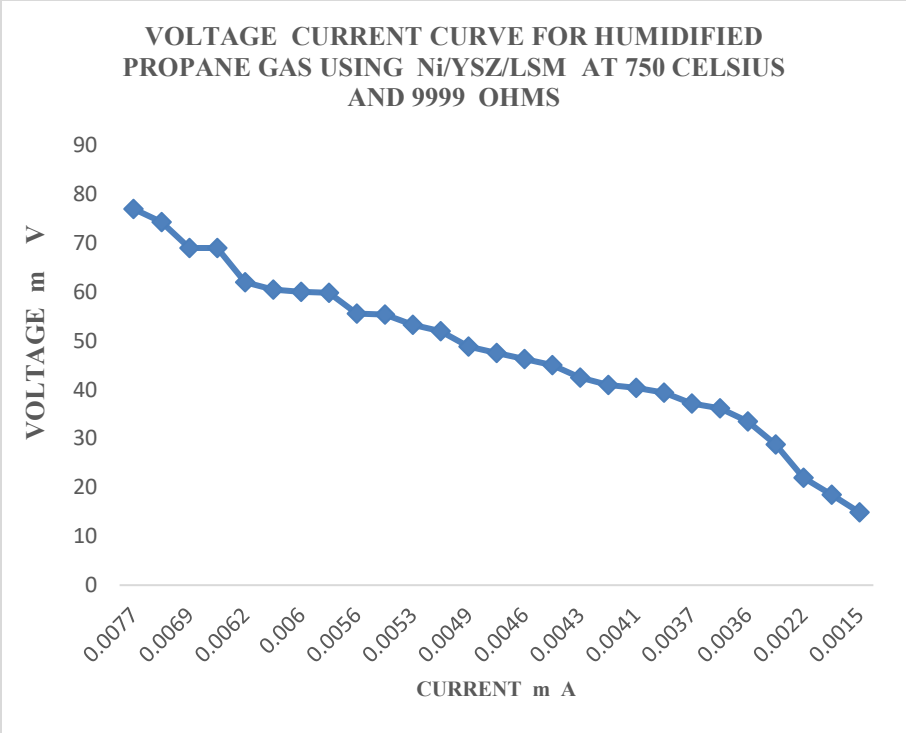

Fig 3.22: Voltage-current plot for humidified C_3H_8 at 9999 Ω

The current obtained after the passage of humidified propane at 99 Ω ranged from 0.089 to 0.046 mA respectively which was greater than the humidified propane ran at 9999 Ω as found in Fig 3.28.

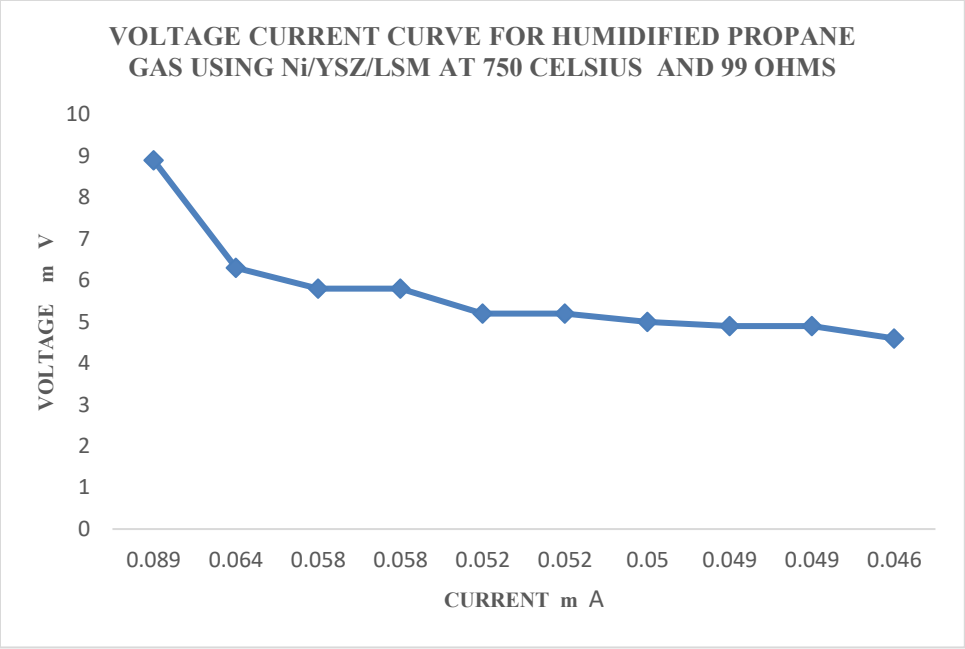

Fig 3.23: Current-voltage plot C_3H_8 for humidified at 99 Ω

When the experiment was completed, the Probostat^{TM} was opened after cooling down to room temperature, and it was observed that large deposits of a black substance and water were formed at the top and bottom of the setup as shown in the images below (Fig 3.24). The black deposit is most likely to be soot. Pang et al. mentioned that hydrocarbon fuel such as propane is composed of C and H atoms, which first under heterolytic cleavage of C-H bonds, followed by formation of C-C bonds.[65]

The formation of the soot can be due to the incomplete steam reforming process for both methane and propane gases, leading to the formation of carbon monoxide. There are a couple of reactions that can occur such as methanation, cracking and reforming of methane that forms soot. The carbon monoxide then dissociates into carbon and gets deposited on the nickel anode. This leads to deactivation of the nickel catalyst by adsorption, encapsulation, cracking and blockage of active sites needed for catalysis. The

irreversible soot formation occurs at higher temperatures, low hydrocarbon to steam ratios, and oxygen carbon ratios.[66]

Hardiman et al. mentioned that the steam carbon ratio should be greater than three, to prevent carbon deposits.[67] Once the active sites are blocked, porosity is minimized, and the flow of air and hydrogen gas is impeded leading to a decrease in voltage and current output. Besides, the deactivation of catalysts during SOFC operations could also be attributed to the sintering of the nickel atoms at high temperatures. This causes agglomeration, and grain growth which creates mechanical failures or drop of overall cell potential.

Fig 3.24: Images of black deposits

POST-ANALYSIS OF Ni/YSZ/LSM CELL USING SEM-EDS

The black substance deposited on the Probostat^{TM} was collected along with the Ni/YSZ/LSM cell and the elemental composition of each of the sample were determined using SEM-EDS as shown in Fig 3.25.

Fig 3.25: Post-analysis of black deposits and Ni/YSZ/LSM

Table 3.5: SEM-EDS analysis of black deposits

ELEMENT	WEIGHT %	ATOMIC %
C	97.09	97.80
O	2.91	2.20

The results from table 3.5 and Fig 3.26 showed the presence of 97.09 % of carbon and this is most likely to represent soot, due to its amorphous form. Soot is an allotrope of carbon formed at high temperatures when hydrocarbons combine with highly reactive species (free radicals) in the flame. Soot is made of nanoparticles of graphite, diamond and black carbon.

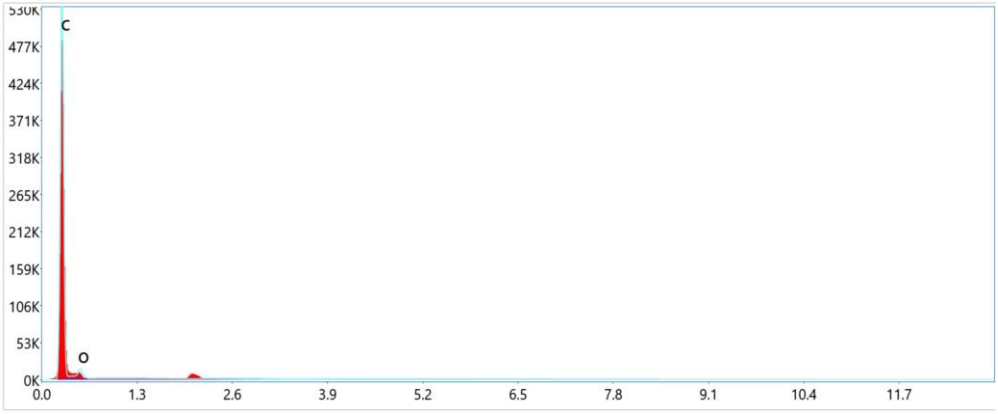

Fig 3.26: SEM-EDS analysis of black deposit

The analysis of the Ni/YSZ/LSM revealed higher amounts of carbon deposits (97.35 %), which means that there was partial steam reforming of the hydrocarbons leading to the enormous deposits of carbon on the anode as shown in Fig 3.27 and table 3.6. The propane gas contributes to higher carbon deposits than methane due to the increase in the number of carbon atoms.

Table 3.6: SEM-EDS analysis of Ni/YSZ/LSM

ELEMENT	**WEIGHT %**	**ATOMIC %**
O	3.22	2.46
C	97.35	97.55

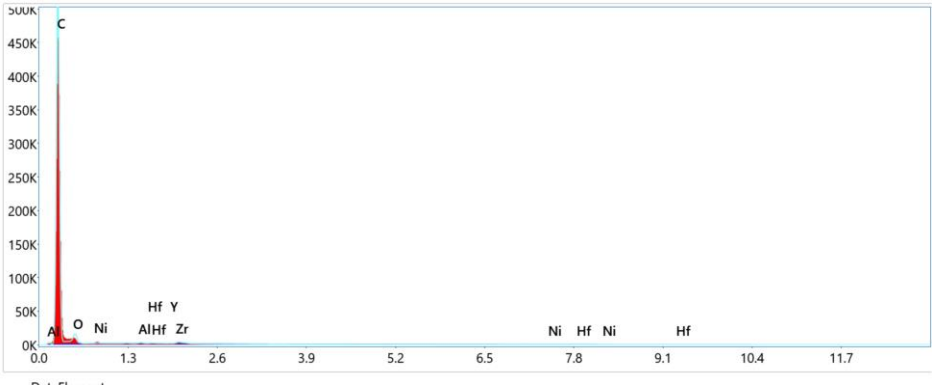

Fig 3.27: SEM-EDS analysis of Ni/YSZ/LSM

CHAPTER FOUR

CONCLUSION

The Ni/YSZ/LSM cell exhibited higher cell performance as compared to the Pt/YSZ/Pt cell after the passage of humidified hydrogen. The voltage was found to be higher when the ammeter was connected in series to the 99 Ω load resistor and the Ni/YSZ/LSM cell.

Scanning Electron Microscopy (SEM), Energy Dispersive Spectroscopy (EDS) and X-Ray Diffraction were conducted on control and coated YSZ cells. The control sample had higher atomic percentages of oxygen (88.90 %), zirconium (9.07 %) and yttrium (1.71 %), which was comparable to the elemental composition listed in the MSDS. Less than 1 mol% of sintering agents, such as aluminum and hafnium, were found in the control YSZ cells. These dopants were added to improve the density and conductivity of 8 mol% YSZ. There were higher atomic percents of carbon (41.00 %), platinum (35.30 %) and oxygen (23.70 %) in the Pt/YSZ/Pt cells. On the other hand, the Ni/YSZ/LSM cell showed 66.78 % of oxygen, 16.35 % nickel, and 13.96 % zirconium.

There was higher cell performance using propane as fuel as compared to methane gas. Images obtained after the experiment showed a black deposit on the anode. Elemental analysis on the black deposit and the nickel anode revealed the presence of 97.09 % and 97.35 % of carbon, respectively. The presence of the black deposits would indicate that water vapor at 0.66 atm was insufficient to prevent carbon deposition via pyrolysis of propane at 750 ºC.

FUTURE DIRECTIONS

I recommend that further analysis involving chronoamperometry and linear weep voltammetric techniques be carried out to determine the adsorption processes and kinetics involved in the carbon deposition at the nickel anode. Impedance spectroscopic analysis can be performed to determine other processes lowering the cell output.

REFERENCES

1. Saidi, M.; Alaedini, A. H.; Tourani, H.K. A review of waste-to-hydrogen conversion technologies for solid oxide fuel cell (SOFC) applications: Aspect of gasification process and catalyst development. *Elsevier Journal of environmental management.* **2023**, 329, 117077. https://doi.org/10.1016/j.jenvman.2022.117077
2. NRDC. Fossil fuels, The dirty Facts. **2022**. https://www.nrdc.org/stories/fossil-fuels-dirty-facts#sec-whatis. Accessed on 1/8/24.
3. Kroyan, Y.; Wojcieszyk, M.; Kaario, O.; Larm, M. Modelling the end-use performance of alternative fuel properties in flex-fuel vehicles. Elsevier, *Journal of energy conversion and management*. **2022**, 269, 116080.
4. US Department of Energy. Fuel cells. Hydrogen and fuel cells technology office. https://www.energy.gov/eere/fuelcells/fuelcells#:~:text=Fuel%20cells%20work%20like%20batteries,)%E2%80%94sandwiched%20around%20an%20electrolyte. Accessed on 1/8/2024.
5. White, L.; Oleksiewicz, A. Fuel Cells. Applications**.2024**. https://publish.illinois.edu/fuel-cells/applications/ 2022. Accessed 1/6/24.
6. Gasik, M. Materials challenges in fuel cells. Materials for fuel Cells. Woodhead Publishing Series in Electronic and Optical Materials. *Science Direct*. **2008** 1-5 https://www.sciencedirect.com/science/article/abs/pii/B9781845693305500014
7. Lai, H.; Harun, N, F.; Tucker, D.; Adams, T.A. Design and Eco-techno-economic Analyses of SOFC/Gas Turbine Hybrid Systems Accounting for Long-Term Degradation. *Elsevier. Computer aided chemical engineering*. **2020**, 48, 415-420.

https://doi.org/10.1016/B978-0-12-823377-1.50070-7https://www.sciencedirect.com/science/article/abs/pii/B9780128233771500707

8. Wei, Z.; Hang, H.Y. Recent progress in design and fabrication of SOFC cathodes for efficient catalytic oxygen reduction. *Elsevier,Catalysis Today*.**2023**, 409,71-86
9. Kim, E.; Kim, H.; Bae, C.; Lee, D.; Moon, J.; Kim, J.; Shin, H. Formation of yttria-stabilized zirconia nanotubes by atomic layer deposition toward efficient solid electrolytes. *Springer, Nano convergence*. **2017**. Article 4. https://nanoconvergencejournal.springeropen.com/articles/10.1186/s40580-017-0127-9
10. Liu, T.; Zhang, X.; Wang, X.; Yu, J.; Li, L. A review of zirconia-based solid electrolytes, *Ionics,* **2016,** 22, (12) 2249–2262. https://doi.org/10.1007/s11581-016-1880-1
11. Heenam, M.M.; Lu, X.; Finegan, D.P.; Robinson, J.; Lacoviella, F.; Bailey, J.J.; Brett D.J.; Shearing, P.R. Evaluating microstructure evolution in an SOFC electrode using digital volume correlation. *Journal of sustainable energy and fuels.* **2018**, 12 (2) 2625-2635. https://doi.org/10.1039/C8SE00292Dhttps://pubs.rsc.org/en/content/articlelanding/2018/SE/C8SE00292D
12. Zhu, B. Solid oxide fuel cells technical challenges and solutions from nano prospects. Nanoscience and technology for energy applications. *International journal of energy research*. **2009**, 33, (13) 1126-1137. https://doi.org/10.1002/er.1600

13. Golkhatmi, S. Z.; Asghar, I.; Lund, P.D. A review on solid oxide fuel cell durability: Latest progress, mechanisms, and study tools. *Elsevier, Renewable and sustainable energy reviews*. **2022.** 161,112339

14. Sasaki, K.; Yoshizumi, T.; Haga, K.; Yoshitomi, H.; Hosoi, T.; Shiratori, Y.; Taniguchi, S. Chemical Degradation of SOFCs. External Impurity Poisoning and Internal Diffusion-related Phenomena. *ECS Transactions*. **2013**, 57 (1) 315-323 10.1149/05701.0315ecst ©The Electrochemical Society.

15. Chen, K.; Liu, S, S.; Guagliardo, P.; Kilburn, M, R.; Koyama, M.; Jianga, S, P.A Fundamental Study of Boron Deposition and Poisoning of $La0.8Sr0.2MnO_3$. Cathode of Solid Oxide Fuel Cells under Accelerated Conditions. .**2015**. 162, (12) 1282-1291. https://iopscience.iop.org/article/10.1149/2.0141512jes/pdf

16. Wang, F.; Yamaji, K.; Cho, T.; D.; Shimonosono, D.; Kishimoto, H.; Brito, M.E.; Horita, T.; Yokokawa, H. Effect of strontium concentration on sulfur poisoning of LSCF cathodes. *Solid State Ionics*, **2012**, 225,157-160

17. Zivak, M. Studying the Effects of Siloxanes on Solid Oxide Fuel Cell Performance. Submitted in Partial Fulfillment of the Requirements for the Degree of Master of Science in the Chemistry Program. Youngstown State University. **2020**. Accessed on 01/10/24

18. Dogho, M.K. Adapting solid oxide fuel cells to operate on landfill gas. Methane passivation of Ni anode. Submitted in Partial Fulfillment of the Requirements for the Degree of Master of Science in the Chemistry Program. Youngstown State University. **2023.** Accessed on 01/10/24

19. Baderuddin, F.K. Microextrusion 3D- printing of solid oxide fuel cell components. **2016,** Doctor of Philosophy in Materials Science and Engineering, Youngstown State University, Department of Chemistry. Accessed on 01/15/24

20. Boldrin, P.; Ruiz-Trejo, E.; Mermelstein, J.; Miguel, J.; Menendez, B.; Reina, T.R.; Brandon, P.N. Strategies for Carbon and Sulfur Tolerant Solid Oxide Fuel Cell Materials, Incorporating Lessons from Heterogeneous Catalysis. *Chem. Rev*, **2016**. 116, 13633−13684. DOI: 10.1021/acs.chemrev.6b00284

21. Aruna, S.T.; Muthuraman, M.; Patil, K.C. Synthesis and properties of Ni-YSZ cermet: anode material for solid oxide fuel cells. *Solid State Ionics* **1998.**11,45–51.

22. Koide, H.; Someya, Y.; Yoshida, T.; Maruyama, T. Properties of Ni/YSZ cermet as anode for SOFC. *Solid State Ionics*. **2000**, 132, 253–260.

23. Wilson, J. R.; Barnett, S. A. Solid oxide fuel cell Ni-YSZ anodes: Effect of composition on microstructure and performance. *Electrochem. Solid State Lett*. **2008**, 11, B181–B185.

24. Laguna-Bercero, M. A. Recent advances in high temperature electrolysis using solid oxide fuel cells: A review. *J. Power Sources*. **2012**, 203, 4–16.

25. Vafaeenezhad, S; Hanifi, A.R; Laguna-Bercero, M.A.; Etsell, T.H.; Sarkar, P. Microstructure and long-term stability of Ni–YSZ anode supported fuel cells: A review. *Materials Futures* **2022**, (1), 042101, 1-34. https://doi.org/10.1088/2752-5724/ac88e7

26. Amezawa, K.; Shindo, Y.; Fujimaki, Y.; Kimura, Y.; Nakamura, T.; Iguchi, F.; Yashiro, K.; Yugami, H.; Kawada, T. Mechanism of Chromium Poisoning in SOFC

Cathode Investigated by Using Pattern Thin Film Model Electrode. *IOP Science. ECS Meeting Abstracts*. **2017**. DOI 10.1149/MA2017-03/1/147

27. Acharya, N.; Sagar, R. $CoMn_2O_4$ and $Cu0.5Co0.5Mn_2O_4$ spinels as efficient protective coating layers on SUS430 for SOFC interconnect. *Ceramics international*, **2023**, 49, 29164 – 29173. https://doi.org/10.1016/j.ceramint.2023.06.197

28. Sakai, N.; Yamaji, K.; Horita, T.; Xiong, Y.; Kishimoto, H.; Yokokawa, H. Effect of Water on Electrochemical Oxygen Reduction at the Interface Between Fluorite-Type Oxide-Ion Conductors and Various Types of Electrodes. *Solid State Ionics*. **2004**, 0167-2738, 174, 103–109.

29. Peng, J.; Zhao, D.; Xu, Y.; Wu, X.; Li, X. Comprehensive Analysis of Solid Oxide Fuel Cell Performance Degradation, Mechanism, Prediction, and Optimization Studies. *Energies* **2023**, 16, 788. https://doi.org/10.3390/en16020788

30. Hackett, G.A. Interaction of nickel-based SOFC anodes with trace contaminants from coal-derived synthesis gas. Dissertation submitted to the College of Engineering and Mineral Resources at West Virginia University in partial fulfillment of the requirements for the degree of Doctor of Philosophy in Chemical Engineering. **2009**, 26. doi:10.1088/1742-6596/463/1/012030

31. Krishnan, G. N. Effect of coal contaminants on solid oxide fuel system performance and service life; SRI International. **2009**. Morgantown, West Virginia

32. Marina, O. A.; Pederson, L. R.; Edwards, D. J.; Coyle, C. W.; Templeton, J.; Engelhard, M.; Zhu, Z. SOFC Operation on Hydrogen and Coal Gas in the Presence

of Phosphorus, Arsenic, and Sulfur Impurities. In 8th Annual SECA Workshop, San Antonio, TX. **2007**

33. Trembly, J. P.; Gemmen, R. S.; Bayless, D. J. The effect of coal syngas containing AsH_3 on the performance of SOFCs: Investigations into the effect of operational temperature, current density and AsH_3 concentration. *Journal of Power Sources* **2007,** 171 (2), 818-825.
34. Ray, E. R.; Maskalick, N. J. Contaminant Effects in Solid Oxide Fuel Cells. In Joint Contractors Meeting: FE/EE Advanced Turbine Systems Conference, FE Fuel Cells, and Coal-Fired Heat Engines Conference. **1993**, 1-10.
35. Li, H. Carbon deposition on Ni/YSZ anode SOFC for direct methane steam reforming". Graduate Theses, Dissertations, and Problem Reports. **2019**, 4070. https://researchrepository.wvu.edu/etd/4070
36. Liang,W.; Yan, H.; Chen, C.; Lin, D.; Tan,K.; Feng, X.; Liu, Y.; Chen, X.; Yang, C.; Shan, H. Revealing the Effect of Nickel Particle Size on Carbon Formation Type in the Methane Decomposition Reaction. *Catalysts*. **2020**, 10, 890 doi:10.3390/catal10080890
37. Watanabe, H.; Ogura, T. Mechanisms of the carbon deposition at the Ni/YSZ interface: A combination study of microscopic observation and first-principles calculation. *International journal of hydrogen energy*. **2022**, (47) 67, 29027-29036. https://doi.org/10.1016/j.ijhydene.2022.06.243
38. Lee, W.Y.; Hanna, J.; Ghoniem, A.F. On the predictions of carbon deposition on the nickel anode of a SOFC and its impact on open-circuit conditions. *Journal of The Electrochemical Society*, **2013**. 160 (2). F94-F105.

39. Boldrin, P.; Ruiz-Trejo, E.; Mermelstein, J.; Menéndez, J.M.B.; Reina, T.R.; Brandon, N.P. Strategies for Carbon and Sulfur Tolerant Solid Oxide Fuel Cell Materials, Incorporating Lessons from Heterogeneous Catalysis. *Chem. Rev*. 2**016**, 116, 13633−13684. DOI: 10.1021/acs.chemrev.6b00284

40. Argyle, M.D.; Bartholomew, C.H. Heterogeneous Catalyst Deactivation and Regeneration: A Review. *Catalysts* **2015**, 5, 145-269 doi:10.3390/catal5010145

41. Wang, Y.; Shen, Q.; Tong, Y.; Zhan, Z. Investigation of Ni^{2+}-doped ceria nanorods as the anode catalysts for reduced-temperature solid oxide fuel cells. *International journal of hydrogen energy*. **2022**, (47), 10, 6827-6836. https://doi.org/10.1016/j.ijhydene.2021.12.012

42. Sakama, S.; Chanthanumataporn, M.; Hanamura, K. Carbon deposition influenced by gas concentration in a Ni/YSZ anode of an internal-reforming solid oxide fuel cell using a detector layer inside the anode. *Elsevier, Journal of Power Sources*, **2022**. 551, 232153. https://doi.org/10.1016/j.jpowsour.2022.232153

43. Butz, B.; Kruse, P; Stormer, H.; Gerthsen, D.; Müller, A.; Weber, A.; Ivers-Tiffee, E. Correlation between microstructure and degradation in conductivity for cubic Y_2O_3-doped ZrO_2. *Solid State Ionics*. **2006**, 177, 3275–3284

44. Hattori, M.; Takeda, Y.; Sakaki, Y.; Nakanishi, A.; Ohara, S.; Mukai, K.; Mukai, Kazuo; Jin-Ho, l.; Takehisa, F. Effect of aging on conductivity of yttria stabilized zirconia. *J Power Sources*.**2004**. 126, 23–27

45. Zalka, D; László, P. On the evolution and application of the concept of electrochemical polarization. *Journal of Solid-State Electrochemistry*, **2020**, 24, 2595–2602. https://doi.org/10.1007/s10008-020-04682-3

46. Kikuchi, R., Murakami, K., Futamura, M, Matsui, T Eguchi, K. Activation Process of Solid Oxide Fuel Cells under Polarization Conditions. *ECS Transactions*, **2007**, 7 (1) 1251-1260. https://iopscience.iop.org/article/10.1149/1.2729226/pdf

47. Virkar, A.V.; Chen, J.; Tanner, C.W.; Kim, J.W The role of electrode microstructure on activation and concentration polarizations in solid oxide fuel cells. *Solid State Ionics*. **2000**, 131, 189-198. www.elsevier.com/locate/ssi

48. US DOE. **2000**. Fuel Cell Handbook, 5th Edition. https://esc.fsu.edu/documents/lectures/SP07/EML4930L13.pdf

49. Wang, R.; Lu, Y.; Ma, Y.; Sun, Z.; Gopalan, S.; Basu, N.S; Pal, U.B. Experimental Validation of Solid Oxide Fuel Cell Polarization Modeling: An LSM YSZ/YSZ/Ni-YSZ Case Study. *Electrochimica Acta*, **2020**, 361, 137052 https://doi.org/10.1016/j.electacta.2020.137052.

50. Kopeliovich, D. Polarization. Knowledge source on materials engineering. *Substances and Technologies* **2023.** https://www.substech.com/dokuwiki/doku.php?id=polarization. Accessed on 05/24/2024.

51. Kalam, S.; Abu-Khamsin, S.A.; Kamal, M.S.; Patil, S. Surfactant Adsorption Isotherms: A Review. *ACS Omega* **2021**, 6, 32342−32348

52. Kulik, D.A. Classic adsorption isotherms incorporated in modern surface complexation models: Implications for sorption of actinides. *Radiochim. Acta*. **2006**, 94, 765–778 DOI 10.1524/ract.2006.94.9.765

53. US EPA. Basic information about landfill gas. **2023**. https://www.epa.gov/lmop/basic-information-about-landfill-gas. Accessed on December 2023.

54. ATSDR. Landfill gas primer- An overview for environmental health professionals. Landfill gas basics.2001 www.atsdr.cdc.gov/hac/landfill/html/ch2.html.Accessed on Sept 2023.

55. United States Environmental Protection Agency. USEPA. Bioreactor Landfills. **2019**. https://www.epa.gov/landfills/bioreactor-landfills. Accessed on 03/10/23.

56. Brodnikovska, I.; Korsunska, N.; Khomenkova, L.; Polishchuk, Y.; Lavoryk, S.; Brychevskyi, M. Brodnikovskyia,Y.; Vasylyev, O. Grains, grain boundaries and total ionic conductivity of 10Sc1CeSZ and 8YSZ solid electrolytes affected by crystalline structure and dopant content. *Materials Today: Proceedings*, **2019** 6, 79–85. doi: https://doi.org/10.1016/j.matpr.2018.10.078

57. Kakani, S.L. Electronics Theory and Applications. *New Age International*. **2005**. 7. ISBN 978-81-224-1536-0

58. Stortelder, J.S. Ionic Conductivity in Yttria-Stabilized Zirconia Thin Films grown by Pulsed Laser Deposition. Master of Science Thesis Faculty of Science and Technology Inorganic Materials Science Mesa, Institute for Nanotechnology Enschede, **2005.** https://www.utwente.nl/en/tnw/ims/publications/former-msc/files/Jetske%20Stortelder.pdf

59. Kilo, M.; Argirusis, C.; Borchardt, G.; Jackson, R.A. Oxygen diffusion in yttria stabilised zirconia—experimental results and molecular dynamics calculations. Phys. Chem. Chem. Phys., 2003, 5, 2219–2224

60. Liu, Q.; Zhang, Q.; Voorhees, P.T.; Barnet, S.B. Effect of direct-current operation on the electrochemical performance and structural evolution of Ni-YSZ electrodes. *J Phys Energy* 2, **2020,** 014006. https://doi.org/10.1088/2515-7655/ab59a6

61. Wagner, N.; Schnurnberger, W.; Müller, B.; Lang, M. Electrochemical impedance spectra of solid-oxide fuel cells and polymer membrane fuel cells, *Electrochim. Acta,* **1998**, 43, 3785–3793, https://doi.org/10.1016/S0013-4686(98)00138-8

62. Montinaro, D.; Contino, A, R.; Dellai, A.; Rolland, M. Determination of the impedance contributions in anode supported solid oxide fuel cells with (La, Sr) (CO, Fe) O_3^- δ cathode, *Int. J. Hydrog. Energy*, **2014**, 39, 21638–21646, https://doi.org/10.1016/j.ijhydene. 2014.09.081.

63. Bai, Y.; Kirvassilis, D; Xu,L; Mavrikakis, M. Atomic and molecular adsorption on Ni (111). Department of Chemical and Biological Engineering, University of Wisconsin-Madison. https://www.osti.gov/servlets/purl/1494812

64. Faes, A.; Jeangros, Q.; Wagner, J. B.; Hansen, T. W.; Van Herle, J.; Brisse, A.; Dunin-Borkowski, R. E.; Hessler-Wyser, A. In situ Reduction and Oxidation of Nickel from Solid Oxide Fuel Cells in a Transmission Electron Microscope. *ECS Transactions,* **2009**. 25(2), 1985-1992. https://doi.org/10.1149/1.3205743

65. Zhang, P.; Yang, Z.; Jin, Y.; Liu, C.; Lei, Z.; Chen, F.; Peng, S. Progress report on the catalyst layers for hydrocarbon-fueled SOFCs. *International journal of hydrogen energy.* **2021**, 30369-39386. https://doi.org/10.1016/j.ijhydene.2021.09.198

66. Sua, X.; Zhanga, F.; Yina,Y.; Tua, B.; Cheng, M. Thermodynamic analysis and fuel processing strategies for propane-fueled solid oxide fuel cell. *Energy*

Conversion and Management.**2020,** 204, 112279.

https://doi.org/10.1016/j.enconman.2019.112279

67. Hardiman, K.M.; Ying, T.T.; Adesina, A.A.; Kennedy, E. M.; Dlugogorski, B.Z.

Chemical Engineering Journal.**2004,** 102, 119–130